

Equilibrium sediment transport by dilute turbidity currents: Comparison of competence-based and capacity-based models

LAWRENCE AMY*  and ROBERT DORRELL† 

*School of Earth Sciences, University College Dublin, Belfield, Dublin 4, Ireland (E-mail: lawrence.amy@ucd.ie)

†Energy and Environment Institute, University of Hull, Hull, HU6 7RX, UK

Associate Editor – Jaco Baas

ABSTRACT

Equilibrium sediment transport is the condition of zero net entrainment and deposition by sediment-transporting flow (i.e. grade or regime). Here criteria for equilibrium sediment transport, or those used as proxies for equilibrium (for example, onset of erosion, onset of particle setting or suppression of turbulence) for dilute, suspended-load-dominated, turbidity currents, are tested against laboratory and natural data. The examined criteria are restricted to those describing flow over a bed of loose particulate material involving non-cohesive sediment. Models include both monodisperse and polydisperse formulations that represent sediment non-uniformity by using a single characteristic grain size or discretization of the grain-size distribution, respectively. Analysis shows that a polydisperse-type flux-balance model, that equates erosional and depositional fluxes and where erosion is related to the power used to lift sediment mass from the bed (the 'Flow-Power Flux-Balance' model) provides predictions most consistent with observational data. Other equilibrium models tested, monodisperse or polydisperse, fail to predict realistic bed slopes and/or flow durations for concentrations, velocities and depths within limits for natural flows. Results of the Flow-Power Flux-Balance model are used to quantify sediment transport fields, equilibrium Shields numbers and slopes for turbidity currents of variable flow and particle properties.

Keywords Equilibrium, erosion, sediment transport, turbidite, turbidity current.

INTRODUCTION

Turbidity currents are an important agent of downslope sediment transport in submarine and lacustrine environments, representing some of the most far-travelled and voluminous sediment transport events on Earth (Meiburg & Kneller, 2010; Talling *et al.*, 2013; Azpiroz-Zabala *et al.*, 2017; Wells & Dorrell, 2021). The behaviour of these currents, the geomorphology they impose on the sea or lake-floor and the stratigraphic architecture they build is fundamentally linked to their ability to maintain sediment in suspension (Kuenen, 1937; Bell, 1942; Middleton &

Hampton, 1973; Parker *et al.*, 1986; Kneller, 2003; Dorrell *et al.*, 2015). Sediment suspension is determined by the hydraulic properties of the flow, but also the character of the sediment in suspension and on the bed, that together dictate the maximum grain size (i.e. flow competence) and maximum amount of sediment (i.e. flow capacity) that can be transported (Kuenen & Sengupta, 1970; Komar, 1985; McLean, 1992; Hiscott, 1994; Dorrell *et al.*, 2013, 2018). Unlike rivers, turbidity currents are driven by their excess density compared with the ambient fluid due to the presence of suspended sediment and, therefore, their flow behaviour is highly

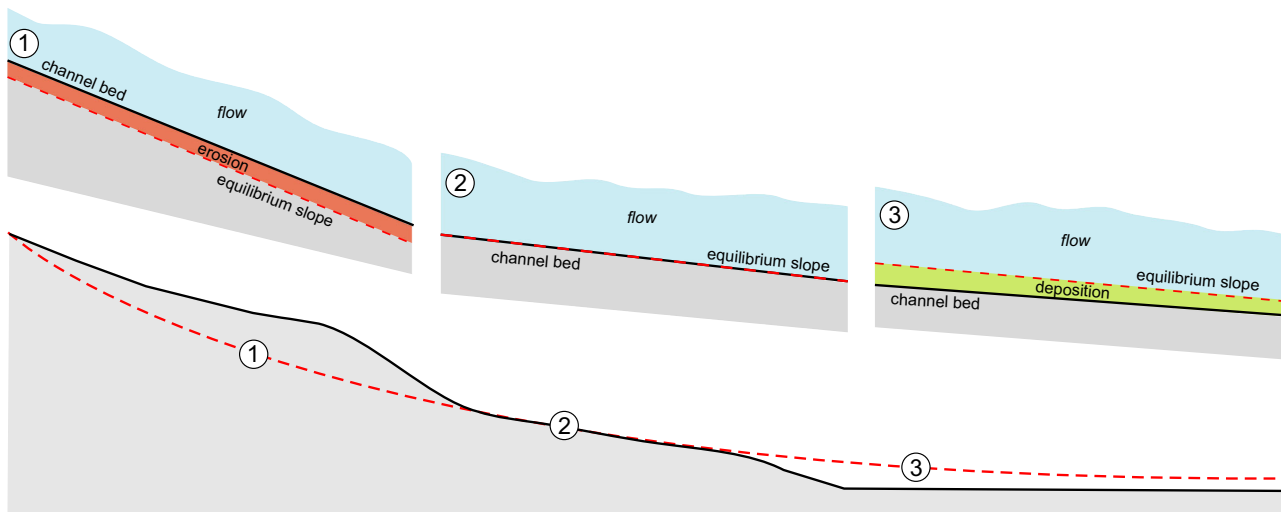


Fig. 1. Schematic diagram showing the instantaneous slope profile (solid line) and the time-averaged graded equilibrium slope (dashed line) a channel theoretically adjusts towards over time through erosion or deposition. Depending upon flow, sediment and substrate conditions, the slope may be out-of-grade where erosion is greater than deposition (1), at grade without net erosion nor deposition (2), or out of grade where deposition is greater than erosion (3).

sensitive to deposition and erosion: deposition may result in collapse of the flow as it loses its driving force, whilst erosion may lead to the flow becoming increasingly erosive or ‘ignitive’ as its driving force increases (Parker, 1982; Parker *et al.*, 1986; Pantin *et al.*, 2011; Halsey *et al.*, 2017).

Assuming an erodible bed of loose sediment, equilibrium describes the condition of zero net erosion and deposition (Smith & Hopkins, 1973; Garcia & Parker, 1991, 1993; Garcia, 2008; Dorrell *et al.*, 2013, 2018; Amy & Dorrell, 2021), and critically defines the boundary between erosional and depositional regimes. This sediment transport state also represents the minimum condition for complete sediment bypass, or ‘bypassing flow’ *sensu* Stevenson *et al.* (2015). In turbidity currents it is questionable whether ‘equilibrium flow’ *sensu stricto* occurs (Halsey *et al.*, 2017), since even under conditions for which steady-uniform flow might be expected, for instance given a constant discharge at the source, entrainment of ambient fluid will cause temporally varied flow (Wells & Dorrell, 2021). However, a stable or pseudo-stable equilibrium between erosion and deposition, or a steady-state equilibrium involving mildly erosive and/or mildly depositional flow may be hypothesized (Halsey *et al.*, 2017). Moreover, under certain regimes of stable stratification where water entrainment is suppressed, flows may also be

able to approximate equilibrium flow conditions (Kneller *et al.*, 2016). Whether equilibrium as defined above is considered to occur within steady-uniform flow or to be a transient phenomenon, both flow and sediment parameters must determine the boundary between erosion and deposition, which in turn dictate equilibrium slope (grade) and equilibrium slope profile (graded slope profile) towards which systems attempt to evolve through time (Fig. 1; Pirmez *et al.*, 2000; Kneller, 2003; Prather, 2003; Janocko *et al.*, 2013). A number of criteria have been developed that describe equilibrium conditions for suspended-load-dominated flows that may be applicable to turbidity currents (Table 1). However, these have received limited validation, largely due to a lack of suitable observational data and, as noted by Stevenson *et al.* (2015), a validated model for accurately predicting equilibrium (or sediment bypass) remains lacking.

The following paper: (i) reviews sediment transport by turbidity currents and criteria for equilibrium; (ii) introduces a new equilibrium criterion based on modification of the flow-power flux-balance (FPFB) model for suspended-load-dominated open channel flow (Dorrell *et al.*, 2018); (iii) compares model predictions with observational data from experimental laboratory flows and modern systems to show that the flow-power flux-balance model provides more robust predictions than other approaches (such as

Table 1. Model formulae for equilibrium, depositional and erosional conditions discussed in this paper.

Model name (basis)	Deposition	Equilibrium	Erosion (or non-deposition)	c^+	E_s	Reference
[1] Rouse (competence)	$w_{sj} > u^*$	$w_{sj} = u^*$	$w_{sj} < u^*$	-	-	Bagnold (1966)
[2] Hiscott (capacity)	$ch > \Gamma$	$ch = \Gamma$	$ch < \Gamma$	-	-	Hiscott (1994)
[3] Hiscott-Kubo (capacity)	$w_{sj} > 0.08u^*$	$w_{sj} = 0.08u^*$	$w_{sj} < 0.08u^*$	$c^+ = r_0C$ $r_0 = 2$	-	Kubo (2004) based on Hiscott (1994)
[4] Leeder (capacity)	$mg\Delta\rho > \rho^*u^*{}^2$	$mg\Delta\rho = \rho^*u^*{}^2$	$mg\Delta\rho < \rho^*u^*{}^2$	-	-	Leeder <i>et al.</i> (2005)
[5] Cantero (turbulence suppression)	$Ri_{*+}\beta_j > K_c$	$Ri_{*+}\beta_j = K_c$	$Ri_{*+}\beta_j < K_c$	-	-	Cantero <i>et al.</i> (2012)
[6] Parker (particle flux)	$\sum_{i=1}^N c_i^+ w_{si} > \sum_{i=1}^N w_{si} E_{si}$	$\sum_{i=1}^N c_i^+ w_{si} = \sum_{i=1}^N w_{si} E_{si}$	$\sum_{i=1}^N c_i^+ w_{si} < \sum_{i=1}^N w_{si} E_{si}$	$c_i^+ = r_0C$ $r_0 = 1 + 31.5(u^*/w_s)^{-1.46}$	$E_s = 0$ for $Z_u < 5$ $E_s = 3 \times 10^{12} Z^{-10} (1 - \frac{Z_c}{Z_u})$ for $5 < Z_u < 13.2$ $E_s = 0.3$ for $Z_u > 13.2$	Parker <i>et al.</i> (1986)
[7] Halsey (particle flux)	$\frac{w_{sj}}{u^*} > \sqrt{\frac{Re_{pl}}{Z_c}}$	$\frac{w_{sj}}{u^*} = \sqrt{\frac{Re_{pl}}{Z_c}}$	$\frac{w_{sj}}{u^*} < \sqrt{\frac{Re_{pl}}{Z_c}}$	$c^+ = r_0C$ $r_0 = 1.6$	-	Halsey <i>et al.</i> (2017)
[8] Flow-power flux-balance model (particle flux)	$c_i^+ w_{si} > \frac{c_i^- E_{si}}{C_m}$	$c_i^+ w_{si} = \frac{c_i^- E_{si}}{C_m} \forall i$ and $\sum_{i=1}^N c_i^- = C_m$	$c_i^+ w_{si} < \frac{c_i^- E_{si}}{C_m}$	$\lambda_i = \int_{\frac{z^+}{h}}^1 (\frac{z^+ - 1 - Z}{h - z^+ Z})^{\frac{w_{sj}}{u^*}} dZ$ where $c_i \equiv \int_{\frac{z^+}{h}}^1 c_i(Z) dZ = \lambda_i c_i^+$	$E_{si} = \frac{\rho^*}{g\Delta\rho h} (\max[u_*^2 - u_{*ci}^2, 0])^{\frac{3}{2}}$	This study based on Dorrell <i>et al.</i> (2018)

simple competence or capacity based criteria for suspended-load-dominated flow; e.g. Komar, 1985; Hiscott, 1994; Leeder *et al.*, 2005) or those implemented within depth-averaged hydraulic models (e.g. Parker *et al.*, 1986; Halsey *et al.*, 2017); and (iv) explores predictions of the flow-power flux-balance model for a number of different aspects of sediment transport. The results have implications for understanding the transport, erosion and deposition of particulate material by low-concentration turbidity currents, and more widely potentially for the prediction of stratigraphic architecture of basin margins, hydrocarbon reservoirs and stratigraphic traps (Amy, 2019), and the storage of pollutants such as microplastics (Kane & Clare, 2019; Pohl *et al.*, 2020a) and organic carbon (Schlünz & Schneider, 2000; Galy *et al.*, 2007; Stetten *et al.*, 2015) in deepwater lacustrine and seafloor environments.

METHODOLOGY

Sediment transport by shear flow

Some key aspects of sediment transport by shear flows over an erodible bed, involving non-cohesive particles, is considered before discussing equilibrium sediment transport models for suspended-load dominated flow. Shear from a flow imparts tangential and normal forces on solid boundaries including particles resting on the bed. The bed shear stress, τ_* [$\text{kg m}^{-1} \text{s}^{-2}$], of a dilute turbidity current flowing down a slope, S [m m^{-1}], may be characterized by the shear velocity, $u_*^2 = \tau_*/\rho$ [ms^{-1}], or by the dimensionless Shields number, that describes the ratio of fluid shear stress to the median gravitational weight of a submerged particle, defined as:

$$\theta = \frac{\tau_*}{g\Delta\rho d_j} \quad (1)$$

where g [ms^{-2}] is the acceleration due to gravity, d_j [m] the characteristic particle diameter and $\Delta\rho = \rho_s - \rho$ [kg m^{-3}] is the difference between particle density and fluid density (Shields, 1936). Herein, unless noted otherwise, the characteristic grain size of suspended-load-dominated transport is taken as $d_j = d_{50}$, the median particle class in suspension, following Bagnold (1966) and Soulsby (1997). Results are presented here using a modified Shields diagram: i.e. Shields number, θ , versus the median phi grain size, $\phi = -\log_2(10^3 d)$ (Krumbein, 1934).

Here a polydisperse system of $i = 1 \dots N$ discrete particle classes is considered. After Soulsby (1997), the critical Shields number, θ_{ci} , for incipient motion of sediment of diameter, d_i , is given by the empirical formula:

$$\theta_{ci} = \frac{0.3}{1 + 1.2D_{si}} + 0.055(1 - e^{-0.02D_{si}}) \quad (2)$$

where the dimensionless particle diameter, $D_{si} = (g\Delta\rho/\rho\nu^2)^{\frac{1}{3}}d_i$, with ν [$\text{m}^2 \text{s}^{-1}$] being the fluid kinematic viscosity. From Eqs 1 and 2, the critical shear velocity is thus $u_{*ci}^2 = \theta_{ci}g\Delta\rho d_i$.

After Soulsby (1997), the particle settling velocity, w_{si} [ms^{-1}], is predicted by an empirical formula covering a combined viscous plus bluff-body drag law for natural irregular sand grains:

$$w_{si} = \frac{\nu}{d_i} \left((10.36^2 + 1.049D_{si}^3)^{\frac{1}{2}} - 10.36 \right) \quad (3)$$

For shear velocities greater than the particle settling velocity, $u_* > \sim w_{si}$, it is commonly considered that entrained particles can be suspended within the flow: the Rouse-based criterion for suspended-load-dominated flow (Rouse, 1937; Bagnold, 1966; Soulsby, 1997). The concentration, $c_i(Z)$, of particulate material carried in suspension at height above the bed, $z = hZ$ [m], where h [m] is flow depth and Z is the dimensionless height above the bed, is given by the Reynolds averaged mass conservation equation (Rouse, 1937):

$$\frac{K}{h} \frac{\partial}{\partial Z} c_i(Z) + w_{si} c_i(Z) = 0 \quad (4)$$

Here the eddy diffusivity, K [$\text{m}^2 \text{s}^{-1}$], describes diffusive mixing of sediment in suspension by turbulent fluid motion as $K = \kappa u_* L f(Z)$, being a function of the: von Kármán's constant, κ [-]; shear velocity, u_* ; a flow mixing length scale, L [m], yielding a mixing length ratio $\lambda = L/h$ (Dorrell & Hogg, 2012); and a structure function, $f(Z)$, that describes the vertical variation in eddy diffusivity with dimensionless flow depth. For open channel flow it is often assumed that the flow mixing length $L = h$, and that the structure function $f(Z) = Z(1 - Z)$. From this the Rouse profile gives the fractional volumetric concentration, $c_i(Z)$ [particle volume/total volume], of each particle class as:

$$c_i(Z) = c_i^+ \left(\frac{Z^+}{1 - Z^+} \frac{1 - Z}{Z} \right)^{\frac{1}{\lambda} \beta_i} \quad (5)$$

where c_i^+ is the volumetric sediment concentration at a dimensionless near-bed height

$Z^+ = 0.01$ (Soulsby, 1997) and $\beta_i = w_{si}/\kappa u^*$ is the dimensionless Rouse number. The total volumetric concentration of sediment in suspension is thus, $c(Z) = \sum_{i=1}^N c_i(Z)$, and the depth-averaged volumetric concentration of sediment, $c = \int_0^1 c(Z) dZ$.

In turbidity currents the velocity maximum is closer to the bed than in open channel flow and thus shear and near-bed turbulent mixing is enhanced (Buckee *et al.*, 2001). Moreover, unlike open channel flow, turbidity currents are characterized by unstable flow ambient-fluid interfaces (Kneller & Buckee, 2000, and references therein). Therefore, although turbulent mixing processes in turbidity currents remain poorly understood (Dorrell *et al.*, 2019; Wells & Dorrell, 2021), it may be assumed that increased shear and mixing towards the lower and upper flow boundaries results in a more uniform eddy diffusivity profile, in comparison to the parabolic profile used in open channel flow models (Soulsby, 1997). A constant eddy diffusivity thus may be considered more appropriate for turbidity currents where $K = \kappa u^* L$, with a flow mixing length-scale $\lambda = L/h = 1/6$ (Dorrell & Hogg, 2012); the corresponding sediment concentration profile is:

$$c_i(Z) = c_i^+ e^{-\frac{1}{\beta_i} Z} \quad (6)$$

Hydrodynamic equilibrium of turbidity currents

For turbidity currents flowing down a slope a balance of forces is implied that allows flow velocity and shear velocity to be related to slope. The dimensionless ratio of gravitational to inertial forces, the bulk Richardson number:

$$Ri = \frac{gRch}{u^2} \quad (7)$$

is a measure of bulk flow stability, where u [ms^{-1}] is the depth-averaged flow velocity and $R = \rho_s/\rho - 1$ the submerged specific gravity of the sediment. Based on the dimensionless bulk Richardson number, the equilibrium slope for equilibrium turbidity currents (i.e. where Ri is constant and there is no net-erosion or net-deposition) is given in terms of a force-balance equation (see, e.g. Abad *et al.*, 2011):

$$RiS = C_d + E_w \left(1 + \frac{1}{2} Ri \right) \quad (8)$$

In the force balance Eq. 8 the gravitational force driving the flow is balanced by (skin)

friction drag at the lower boundary, C_d [-], and drag induced by momentum lost to entrained ambient fluid (which increases the height of the centre of mass of the flow). Model results are sensitive to the drag coefficient. Assuming highly turbulent natural flows (Reynolds number, $Re > 10^3$), laboratory data suggest that the skin drag coefficient is typically of order 10^{-3} (Cossu & Wells, 2012; Wells & Dorrell, 2021). Field measurements of natural density currents also lead to estimates of order 10^{-3} (Cossu & Wells, 2012). In this work a basal drag coefficient, $C_d = 0.0025$ is assumed (Wells & Dorrell, 2021). The dimensionless ratio for ambient fluid entrainment is, to leading order:

$$E_w = \frac{a}{b + Ri} \quad (9)$$

where the empirical constants $a = 0.00153$ and $b = 0.0204$ (Parker *et al.*, 1986; Abad *et al.*, 2011). It should be noted that the controls on ambient-fluid entrainment are complex (Wells & Dorrell, 2021), depending on the Richardson number, but also the Reynolds number (Peltier & Caulfield, 2003; Caulfield, 2021) and the gradient Richardson number (Stacey & Bowen, 1988; Kneller & Buckee, 2000; Sequeiros *et al.*, 2010; Kneller *et al.*, 2016). For simplicity, this study relies on the leading order assumption, Eq. 9, that has been employed previously (e.g. Parker *et al.*, 1986; Abad *et al.*, 2011).

Morphodynamic equilibrium of turbidity currents

Various models have been used to describe equilibrium conditions of turbidity currents. These models have been implemented within modified-Chezy, box (integral), depth-averaged (shallow-water) and depth resolved (Navier-Stokes) type turbidity current models (for useful summaries of turbidity current model types refer to Kneller & Buckee, 2000; Meiburg & Kneller, 2010; Meiburg *et al.*, 2015). A distinction may be made between equilibrium criteria that consider: (i) what material can be held in suspension, and does not account for sediment entrainment; and (ii) those that assess the balance between sediment entrainment and deposition. Here equilibrium models are discussed covering a variety of approaches, noting that this represents only a subset of proposed models and specific model assumptions employed within previous studies (Table 1). The final model discussed – the flow-power flux-balance model – is

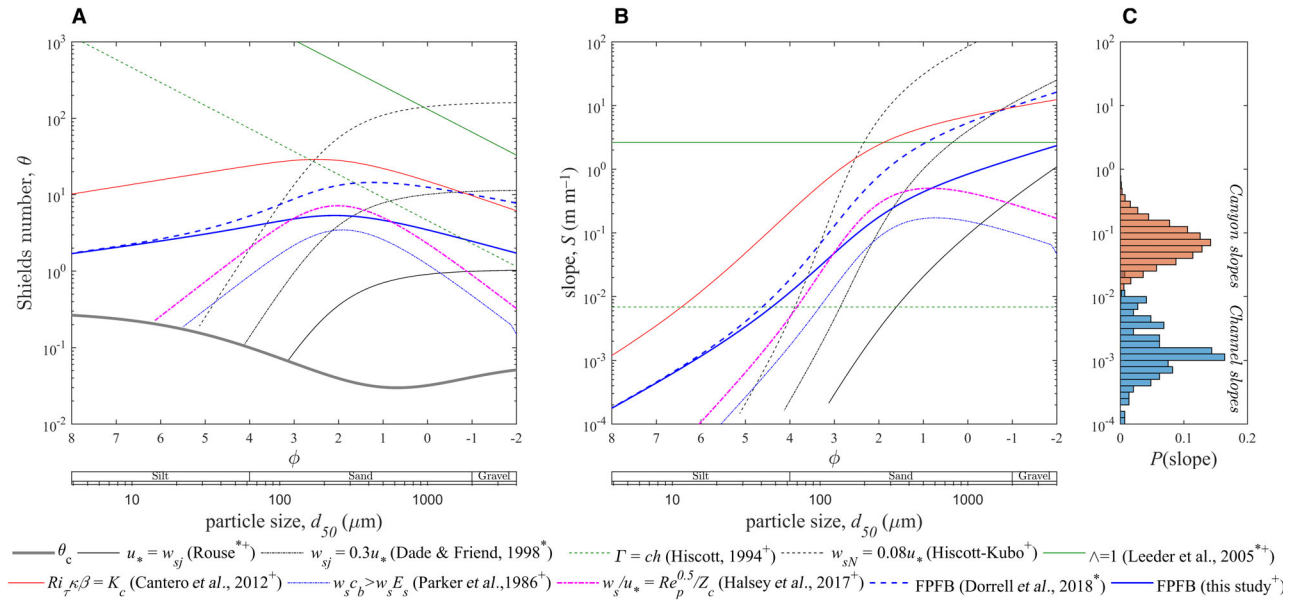


Fig. 2. Comparison of (A) equilibrium Shields number and (B) equilibrium slope predicted by equilibrium models for turbidity currents (⁺), and for comparison open channel flows (^{*}), versus median particle size. Model results assume a flow depth, $h = 50$ m, concentration, $c = 0.1\%$, and a uniform particle size. (C) Probability distribution of slopes for submarine canyons and channels based on data reported by Harris & Whiteway (2011) and Konsoer *et al.* (2013), respectively.

adapted here for application to turbidity currents based on the model of Dorrell *et al.* (2018). A comparison of these models highlights the markedly different model predictions for equilibrium Shields numbers and slope, and thus what particle sizes could be transported on natural submarine slopes (Fig. 2). Comparisons are made assuming flows of water transporting silica particles, where $\rho = 1000 \text{ kg m}^{-3}$, $\rho_s = 2650 \text{ kg m}^{-3}$ and $\nu = 1 \times 10^{-6} \text{ m}^2 \text{ s}^{-1}$. The models considered here assume and are limited to relatively dilute turbidity currents in which particle concentration and cohesive effects are negligible. They thus do not describe phenomena, such as hindered settling (Richardson & Zaki, 1954; Davies, 1968), particle flocculation and gelling (Buscall, 1990; Kranenburg, 1994; Amy *et al.*, 2006), and turbulent enhancement or dampening (e.g. Baas *et al.*, 2009), that may occur within relatively high concentration or clay-rich flows. Furthermore, many models assume a uniform grain size (i.e. monodisperse models). In the case of non-uniform sediment sizes, monodisperse models use a single representative grain size in order to characterize the settling velocity, often the mean or median value (Rouse, 1937; Einstein, 1950; van Rijn, 1984; Garcia & Parker, 1991; McLean, 1992; Zyserman & Fredsoe, 1994; Camenen & Larson, 2008). It is unclear what, if

any, grain-size percentile is appropriate to utilize in monodisperse models for a robust description of suspension dynamics of poorly sorted mixtures (Bagnold, 1966; Komar, 1985; McLean, 1992). Here the authors have chosen to consistently use the median particle size of suspended material for the characteristic grain size, $d_j = d_{50}$, and characteristic settling velocity, w_{sj} (McLean, 1992; Dorrell *et al.*, 2018). Alternative percentile particle sizes may be chosen, however, they may all be criticized as failing to describe the dynamics of the finer or coarser particle classes, respectively (Komar, 1985; McLean, 1992; Dorrell *et al.*, 2018).

Rouse competence criterion

Rouse-based criteria are derived from the Rouse equation for suspended sediment distribution in a shear flow (Rouse, 1937). It may be argued that flows should be competent to support sediment of a specific size in suspension if their particle settling velocity is smaller than the upward turbulent component of velocity (Rouse, 1937; Bagnold, 1966). Given a fixed smooth boundary, the upward velocity component of turbulent flow is similar in magnitude to the shear velocity (Leeder *et al.*, 2005, and references therein). Thus, as a first approximation flows may be considered competent to suspend particles given $u_* > \sim w_s$ (i.e.

the Rouse criterion). The Rouse criterion is widely used to define the boundary between bedload-dominated and suspended-load-dominated transport fields, and for turbidity currents has been applied for the onset of deposition (e.g. Komar, 1985; Mulder *et al.*, 1997) and equilibrium conditions (Kneller, 2003).

Defining a specific value for the ratio of particle settling velocity to shear velocity, $B = w_s/u_*$, that signifies suspension is problematic. The bedload-dominated to suspended-load-dominated regime boundary is by nature transitional and hence difficult to define (Parsons *et al.*, 2015). Values for $B = w_s/u_*$ proposed to signify the regime boundary vary from $0.4 < B < 1.8$ (summarized by Komar, 1980; Burr *et al.*, 2006). This variation in B may reflect differences in the (assumed or actual) asymmetry of vertical turbulent velocities (Bagnold, 1966), ratio of diffusive mixing of momentum to diffusive mixing of sediment, i.e. the turbulent Schmidt number (van Rijn, 1984; Bennett *et al.*, 1998; Cellino & Graf, 1999), and the different definitions applied for the threshold of suspension. The Rouse criterion is evaluated herein taking an upper and lower value of B for the threshold of suspension as:

$$B = \frac{w_{sj}}{u_*} = 1 \quad (10a)$$

and;

$$B = \frac{w_{sj}}{u_*} = 0.3 \quad (10b)$$

that may be considered to cover the range in the required shear stress for suspended-load dominated flow. van Rijn (1984) and Niño *et al.* (2003) concluded that $w_s = u_*$ (Eq. 10a) defines an upper limit of the bed shear stress at which a concentration profile of suspended sediment starts to develop. Dade & Friend (1988) adopted a criterion of $B \leq 0.3$ (Eq. 10b), somewhat lower than most other studies, for predominantly suspended-load-dominated sediment transport. A value of $B = 0.3$ was also found to provide a best fit to data for equilibrium open channel flows (Dorrell *et al.*, 2018). The two relations, Eqs 10a and 10b, are shown in Fig. 2. The critical shear stress using these relations is directly governed by the particle settling velocity, with a change in the gradient of proportionality between particle settling regimes. Assuming $B = 1$ in order to predict equilibrium Shields numbers and slopes gives relatively low values compared to the other models discussed here

(Fig. 2). Applying $B = 0.3$ (Eq. 10b) suggests substantially higher values, comparable to other models for coarser grain sizes ($\phi > 2$) (Fig. 2).

Hiscott capacity criterion

A significant limitation of the Rouse criterion for suspension, as previously discussed by others (e.g. Hiscott, 1994; Leeder *et al.*, 2005; Stevenson *et al.*, 2015), is that the flow capacity (i.e. amount of mass a flow can suspend) is not taken into account. Flow capacity has been inferred to be the most critical factor controlling deposition from sediment gravity flows, notably given the relationship between the excess density and potential energy of currents, with some arguing that flows are likely to be at or near capacity, notably at the onset of deposition (Hiscott, 1994). Hiscott (1994) employed the concept of capacity-driven deposition, where sedimentation occurs when the amount of suspended particles exceeds the capacity of the flow, $ch > \Gamma$. The flow capacity (concentration) is defined by:

$$\Gamma = p_z c^+ h \quad (11)$$

where p_z is the integral of the relative concentration (c/c^+) over the dimensionless flow depth, estimated by Hiscott (1994) using an analytical approximation for the Rouse profile, Eq. 5. This approach has been adapted to model polydisperse turbidity currents (e.g. Kubo, 2004; Kubo *et al.*, 2005; Teles *et al.*, 2016). Since a relation for the reference concentration c^+ was not specified to close Eq. 11, the procedure employed by Hiscott (1994) does not allow for an independent analysis of equilibrium shear stress. Instead, an initial value for capacity, Γ , was imposed by Hiscott (1994), assuming a flow depth, density and slope and solving for the bed shear stress, $\tau_* = \rho g' h S$, where the reduced gravity of the current, $g' = g(\rho_c - \rho)/\rho$ [ms^{-2}] and ρ_c [kg m^{-3}] is the density of the current. This methodology, however, imposes no limit on the near-bed concentration resulting in unrealistically high values of c^+ for high β values. Moreover, the bed shear stress relation unsatisfactorily yields an equilibrium u_* invariant of particle size, corresponding to a Shields relationship that follows, $\theta \propto d_{50}^{-1}$ (Fig. 2). Hiscott's (1994) approach is thus not considered further in the present work.

Alternatively, imposing a limit on c^+ , the condition $\Gamma = ch$ may be found to be a function of w_{sN}/u_* , where w_{sN} denotes the settling velocity of the largest particle size. For instance, assuming

$c_i^+ = r_0 c_i$ where $r_0 = 2$, yields the critical condition for the onset of settling, $\Gamma = ch$, equivalent to $w_{sN}/u_* \approx 0.08$ (Kubo, 2004); noting here, assuming a constant value of the coefficient, r_0 , neglects the effect of particle size-dependent stratification on the near-bed particle size concentration. Thus, making these assumptions to solve Eq. 11 provides the same functional relationship for equilibrium as the Rouse criterion (Eq. 10), albeit providing higher values for Shields number given $w_{sj}/u_* \approx 0.08$, herein referred to as the Hiscott-Kubo criterion (Fig. 2).

Leeder capacity criterion

Leeder *et al.* (2005) proposed an alternative capacity-based criterion for the maintenance of suspension based on the ratio of fluid vertical turbulent momentum to suspended solid momentum, expressed in terms of shear velocity as:

$$\Lambda = \frac{\rho u_*^2}{m(\rho_s/\rho - 1)g} \geq 1 \quad (12)$$

where m [kg m^{-2}] is the mass of suspended sediment per unit area. Here Eq. 12 uses the dimensionless form provided by Stevenson *et al.* (2015). This criterion, however, like the approach used by Hiscott (1994), does not account for the effect of particle size. Given the dependency of both particle stratification and the near-bed particle concentration on particle size, flow capacity must also be influenced by particle size (as discussed by Dorrell *et al.*, 2013). Given the same suspended mass, therefore, Λ also unsatisfactorily results in a constant value for shear velocity with particle size where, $\theta \propto d_{50}^{-1}$, and a constant value for slope (Fig. 2).

Cantero turbulence suppression criterion

Cantero *et al.* (2012) derived a criterion for the onset of turbulence suppression, that they argue can operate in dilute ($c < \sim 1\%$) turbidity currents at the base of a flow due to flow stratification, based on direct numerical simulations:

$$\frac{Ri_\tau \kappa \beta_j}{K_c} > 1 \quad (13)$$

where the shear stress Richardson number, $Ri_\tau = (g(\rho_s/\rho - 1)ch)/u_*^2$, and the critical value beyond which suspended sediment extinguishes turbulence $K_c = 0.041 \ln(u_* h/\nu) + 0.11$. For this criterion, values greater than unity imply the onset of stratification-related turbulence suppression and thus implies deposition. This model predicts relatively high values of equilibrium

Shields numbers that have a relatively weak dependency on particle size with a maxima at $d_{50} \sim 2\phi$ (Fig. 2). It may be noted that this criterion is based on a simplified model of a turbidity current without ambient water entrainment, and does not explicitly account for the dependency of turbulence suppression on particle size (Bennett *et al.*, 1998), nor the potential for regimes under which particles may cause turbulence enhancement (Elghobashi, 1994).

Parker and Halsey flux-balance models

Many models have terms for the downward depositional flux of particles near the bed, $w_s c_i^+$, and the upward erosive flux of particles from the bed, $E_s c_i^+$, where E_s is a dimensionless coefficient of bed sediment entrainment (Garcia & Parker, 1991). Equilibrium conditions are thus given when there is a balance in fluxes. This approach has been utilized for instance within depth-averaged turbidity current models (e.g. Parker *et al.*, 1986; Zeng & Lowe, 1997; Kubo, 2004; Halsey *et al.*, 2017), where sediment entrainment is commonly modelled as:

$$E_{si} = \frac{AZ_{ui}^5}{1 + \frac{A}{0.3}Z_{ui}^5} \quad (14)$$

where the dimensionless tractive stress;

$$Z_{ui} = \frac{u_*}{w_{si}} Re_{pi}^n \quad (15)$$

the particle Reynolds number $Re_{pi} = \sqrt{Rg} d_i^{3/2}/\nu$ and the constant $A = 1.3 \times 10^{-7}$ (Garcia & Parker, 1991). Erosion occurs if $Z_{ui} > Z_c$, where Z_c is the critical value for the onset of significant suspension and limited by a maximum value, Z_m (Parker *et al.*, 1986; Garcia & Parker, 1991; Garcia & Parker, 1993). Results applying the model of Parker *et al.* (1986) to solve for the equilibrium condition:

$$\sum_{i=1}^N c_i^+ w_{si} = \sum_{i=1}^N w_{si} E_{si} \quad (16)$$

are shown in Fig. 2, using their original assumptions, where $c_i^+ = r_0 c_i$, $r_0 = 1 + 31.5(u_*/w_{si})^{-1.46}$, $E_{si} = 0$ for $Z_{ui} < Z_c$, $E_{si} = 3 \times 10^{12} Z_{ui}^{-10} (1 - (Z_c/Z_{ui}))$ for $Z_c < Z_{ui} < Z_m$, $E_{si} = 0.3$ for $Z_{ui} > Z_m$, $n = 0.5$, $Z_c = 5$ and $Z_m = 13.2$. This suggests a markedly different form of equilibrium compared to other models discussed so far (Fig. 2). Based on the Parker *et al.* (1986) approach, Halsey *et al.* (2017) proposed that equilibrium may also be approximated by the onset of erosion described by:

$$\frac{w_{sj}}{u_*} = \frac{\sqrt{Re_{pj}}}{Z_c} \quad (17)$$

assuming $Z_c = 19$, which provides a similar result to the Parker *et al.* (1986) model (Fig. 2).

Flow-power flux-balance model

Dorrell *et al.* (2018) proposed a theoretically derived closure for sediment erosion and thus the equilibrium criterion for open channel flow, where depositional flux balances the erosional flux of particles. This theoretically derived model has been shown to provide a good fit to open channel flow data by Dorrell *et al.* (2018). Further, the cubic dependence on shear velocity has been independently reproduced using empirical multi-variant regression analysis of a large dataset for sediment transport by de Leeuw *et al.* (2020). Equation 6 is used here to modify this model for application to turbidity currents (see also Crisóstomo-Figueroa *et al.*, 2020). The criterion is derived from a one-dimensional sediment suspension model, Eq. 4, for flow over an erodible substrate where particles are freely exchanged between the flow and the bed via an ‘active layer’ (Hirano, 1971). Entrainment rate as modified by the active layer and bed concentration is given by $c_i^-/c_m E_{si}$, where c_i^- is the individual particle class concentration for the active layer and $c_m = 0.6$ the bed packing concentration (Dorrell & Hogg, 2010). The parameter E_{si} denotes a flow-depth dependent entrainment function, describing the power required to lift sediment into suspension (Dorrell *et al.*, 2018), given by:

$$E_{si} = \frac{\varepsilon \rho}{g \Delta \rho h} (\max[u_*^2 - u_{*ci}^2, 0])^{\frac{3}{2}} \quad (18)$$

where $\varepsilon = 13.2$ is an empirical parameter describing entrainment rate, based on a best fit to ten separate experimental datasets for equilibrium open channel flows (Dorrell *et al.*, 2018). Deposition rate is given by the near-bed concentration of the suspension assuming $Z^+ = 0.01$ and particle settling velocity, $c_i^+ w_{si}$. Equilibrium flow is thus defined as satisfying:

$$\frac{c_i^-}{c_m} E_{si} = c_i^+ w_{si} \nabla_i \quad \text{and} \quad \sum_{i=1}^N c_i^- = c_m \quad (19)$$

for all particle class sizes. The flow-power flux-balance model takes into account both the competence and capacity of the flow, and also accounts for particle size distribution effects, that

have a marked influence on equilibrium conditions (McLean, 1992; Dorrell *et al.*, 2013; Amy & Dorrell, 2021). Shields numbers and equilibrium slopes predicted by this model follow a similar form to those of the Cantero *et al.* (2012) model (Fig. 2). For comparison the open channel flow formulation of the flow-power flux-balance model is also shown in Fig. 2. The results of these formulations depart for particle sizes $d_{50} < 6\phi$ with the deviation becoming greater with increasing particle size.

RESULTS: MODEL PREDICTIONS VERSUS OBSERVATIONAL DATA

Comparison of equilibrium flow models with laboratory data

In this section, predicted model equilibrium Shields numbers are compared to data from laboratory flows. Ideally observational data would come from natural flows and whilst there is a growing amount of information for monitored flows (see Talling *et al.*, 2013; Clare *et al.*, 2020; and references therein), these generally have sparse concentration measurements and it is usually unknown whether flows are erosional or depositional at the time of measurement. Therefore, data are used from selected published experimental studies for sustained laboratory turbidity currents in straight channels with suitable flow concentration, velocity and particle size distribution measurements (Gray *et al.*, 2005, 2006; de Leeuw *et al.*, 2018; Sequeiros *et al.*, 2018; Eggenhuisen *et al.*, 2019; Pohl *et al.*, 2020b). Whilst there are a large number of other laboratory studies these are unsuitable for the present analysis, since they involve fully or partially solute driven currents, currents with high particle concentrations (>10%), highly unsteady or non-uniform flow due to input setup or tank geometry, or lack the necessary flow measurements. The six laboratory studies used here include data for experiments with depositional, decelerative (implying depositional), non-depositional ‘bypassing’ (implying equilibrium or erosional) and accelerative (implying erosional) flow conditions. All experimental currents have bulk concentration $c < 11\%$ and Reynolds numbers $Re = uh/\nu > 7000$. The flows reported by de Leeuw *et al.* (2018), Eggenhuisen *et al.* (2019) and Pohl *et al.* (2020b) have relatively high bulk concentrations (7–10%), such that particle–particle interactions may contribute

or be the dominant sediment support mechanism near the bed.

The depth-averaged properties of laboratory flows were calculated using reported measured vertical profiles of concentration and velocity within the body of currents (see Appendix A2). The Shields numbers for reported laboratory currents were calculated using the bulk Richardson number dependent force balance for quasi-equilibrium flow Eq. 8 (see Appendix A3). Figure 3 shows observed Shields numbers for laboratory flows, θ_o , compared to predicted model equilibrium values, θ_{ep} , from the equilibrium models discussed above. Assessment of the models may be made based on whether models predict the correct sediment transport regimes (i.e. depositional, $\theta_o < \theta_{ep}$ versus erosional $\theta_o > \theta_{ep}$). Using this approach shows that the Rouse, Leeder, Cantero and Parker models do not effectively distinguish erosional and depositional experimental flows. The Rouse criterion, Eq. 10, provides substantially lower predicted θ_{ep} values compared to observed θ_o , placing all or most experiments into the erosional field (Fig. 3A). The Leeder and Cantero models predict all flows to be in the depositional regime, with the exception of high concentration bypassing flows – data from de Leeuw *et al.* (2018), Eggenhuisen *et al.* (2019) and Pohl *et al.* (2020b) – for the Cantero model where $\theta_o \approx \theta_{ep}$ (Fig. 3C and D). The Hiscott, Halsey and flow-power flux-balance models (Fig. 3B and E) make adequate predictions for sediment transport regime in all or most cases.

Comparison with natural equilibrium slopes

As a further test of model performance, equilibrium conditions predicted by models are compared with information from the Madeira Channel System, which uniquely offers a dataset where recent (Quaternary) flows are inferred to have bypassed their entire sediment load, without leaving a deposit nor substantially eroding the channel and where the particle size distribution carried by flows may be estimated (Stevenson *et al.*, 2013). Slopes for the Madeira Channel estimated from the modern sea floor bathymetry are $ca\ 10^{-3}\ m\ m^{-1}$ and the bulk particle size distribution of bypassed material may be assessed based on the large number of cores taken from the distal Madeira Abyssal Plain [Stevenson *et al.* (2014): see Appendix A4].

It is assumed that flow within the Madeira Channel System involves suspended-load dominated currents; this inference has been made by

Talling *et al.* (2007) and Stevenson *et al.* (2013). It has also been speculated that bypassing currents within the Madeira Channel System may have transformed from higher-concentration debris flows traversing the Agadir basin-plain (Talling *et al.*, 2007). Whilst there are no deposits recognized in the channel axis, the character of deposits located on the channel margin suggest deposition from flow with relatively low sediment concentrations (Stevenson *et al.*, 2013), although higher concentration flow would be expected within the channel thalweg (Peakall *et al.*, 2000; Eggenhuisen *et al.*, 2019). Whilst flow thickness is unknown, the depositional record suggests that these flows had minimum depths greater than the channel depth, i.e. $h > 20 - 30\ m$ (Stevenson *et al.*, 2013). Comparison of slope and median grain size estimated for the Madeira Channel flows by equilibrium models is shown in Fig. 4A. Here, model inputs were chosen in order to provide the broadest spread of results given variable flow depth, concentration and particle standard deviation within expected natural limits. This analysis separates models into those that either under-predict slope (Rouse model), over-predict slope (Cantero model) and those where observational data fall within the range of model results (all other models). The under and over-prediction of slope made by the Rouse and Cantero models are consistent with their misprediction of laboratory current Shields numbers (Fig. 3).

Predicted flow concentration, depth and duration

The equilibrium models are next further evaluated based on their respective predictions of flow concentration, depth and duration for bypassing flows of the Madeira Channel System. Figure 4B shows computed equilibrium slopes for varying flow depths and concentrations, assuming a median particle size $\phi = 5$ and for polydisperse models a phi log-normal particle size distribution with a standard deviation $\sigma = 1.26$ (average values for the Madeira Abyssal Plain deposits). As may be seen, to satisfy a slope appropriate for the Madeira Channel of $ca\ 10^{-3}$ (red contour line), models predict substantially different ch values. The Hiscott-Kubo, Parker and Halsey models predict lower values of ch compared to the flow-power flux-balance model. The Rouse, Cantero and Parker models do not provide a solution for $ca\ 10^{-3}$ equilibrium slope in the limits of c and h considered.

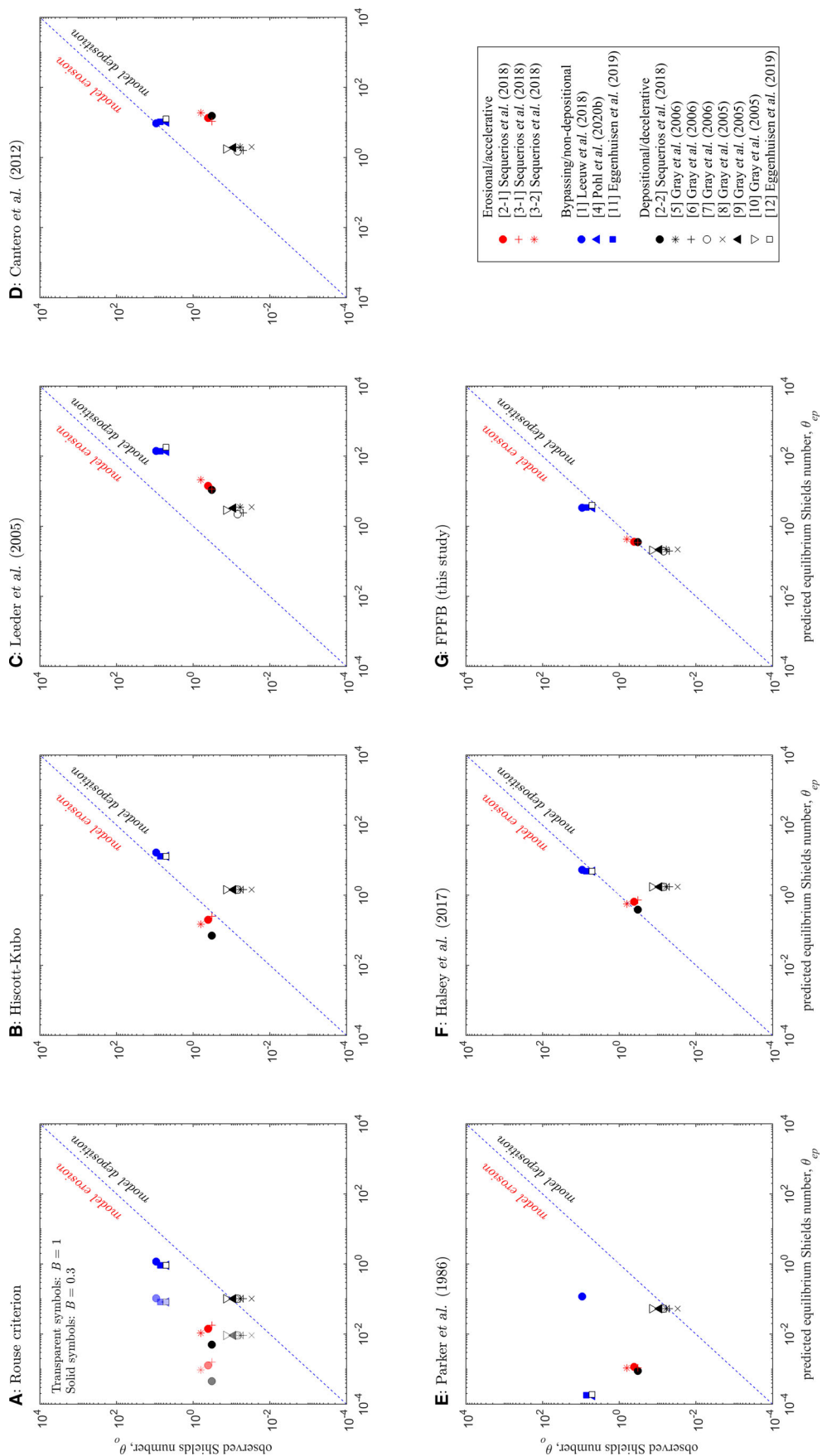


Fig. 3. Comparison of predicted model equilibrium Shields number versus Shields number for sustained laboratory turbidity currents exhibiting erosional/accelerative flow (red symbols), bypassing/non-depositional flow (blue symbols) and decelerative/depositional flow (black symbols) conditions. See Table A1 for further details regarding experimental flow parameters.

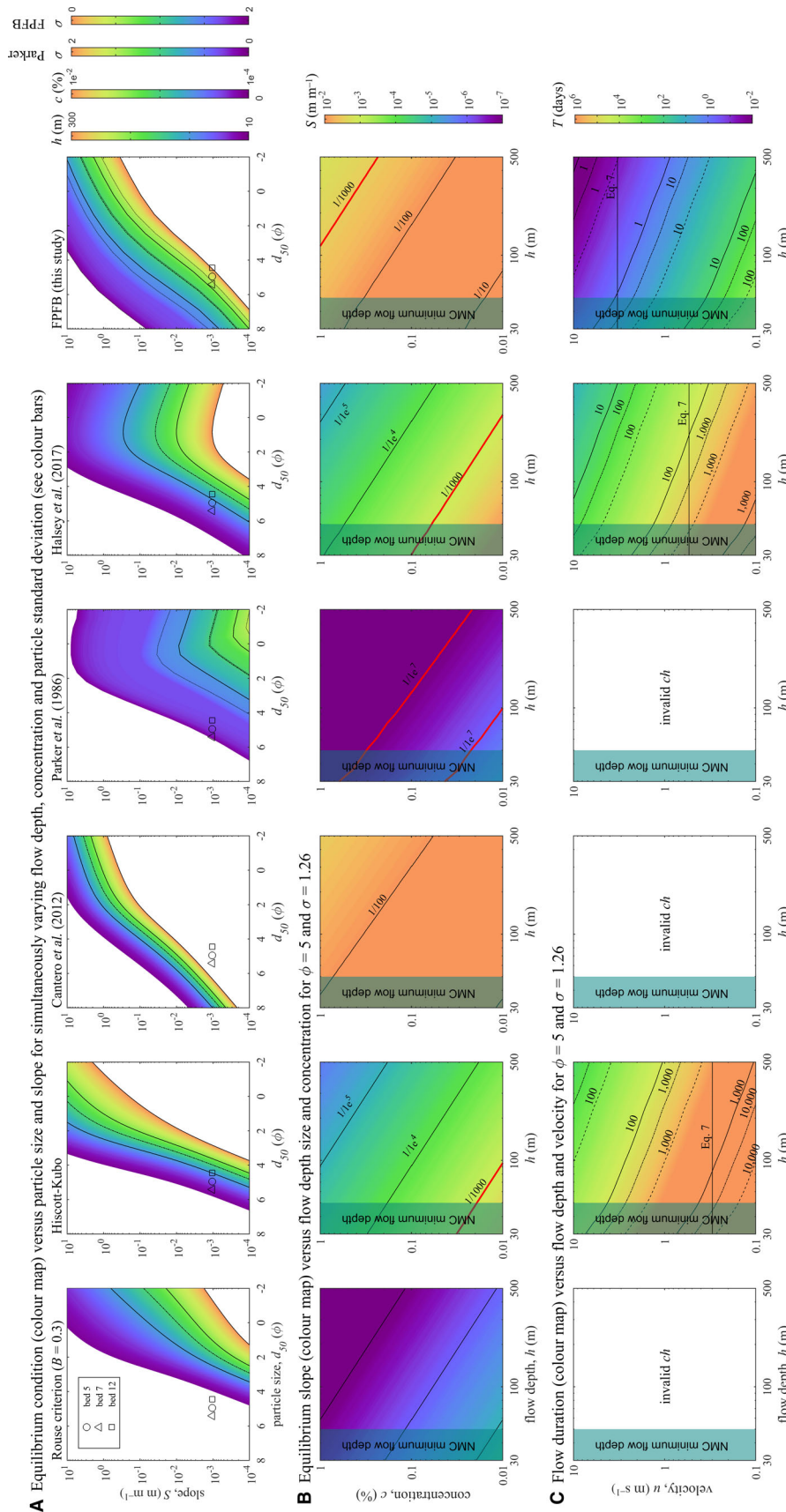


Fig. 4. Equilibrium model predictions. (A) Equilibrium slope, S , versus median particle size, d_{50} , for flows of variable flow depth, h , concentration, c [%], and particle standard deviation, σ , indicated by colour scales and the contour lines —, - - -, · · ·, · · ·, respectively. Note flow depth, concentration and particle standard deviation are varied simultaneously in order to show the widest predicted range in equilibrium slopes. Symbols indicate slope-particle size values for Beds 5, 7 and 12. (B) Equilibrium slope (colour scale) versus flow depth and concentration assuming $d_{50} = 5\phi$, $\sigma = 1.26$. The Madeira channel slope is ca 10^{-3} m m $^{-1}$ (—). (C) Flow duration (colour scale) versus flow depth and mean velocity for beds 5 (—), 7 (---) and 12 (---) of the Madeira channel flows assuming $d_{50} = 5\phi$ and $\sigma = 1.26$. Shaded boxes indicate estimated minimum flow velocity (— horizontal line). Shaded boxes indicate estimated minimum flow depths in the North Madeira Channel (NMC).

Table 2. Summary of model performance where colours indicate: (i) green for correct model predictions; (ii) yellow for partially correct model predictions and; (iii) grey for incorrect model predictions. Model correctness is judged in terms of how well models predict observational data and whether models predict physical parameters within the limits considered reasonable for natural low-concentration turbidity currents.

Model	Comparison to laboratory current flow regimes (Fig. 3)	Prediction of Madeira Channel flow equilibrium (Fig. 4A)	Prediction of Madeira Channel slope (Fig. 4B)	Prediction of Madeira Channel flow durations (Fig. 4C)
Flow-Power	Green	Green	Green	Green
Flux-Balance	Green	Green	Green	Green
Hiscott-Kubo	Green	Green	Green	Green
Halsey	Yellow	Grey	Grey	Grey
Parker	Grey	Grey	Grey	Grey
Rouse with $B = 0.3$	Grey	Yellow	Grey	Grey
Rouse with $B = 1.0$	Grey	Grey	Grey	Grey
Cantero	Grey	Grey	Grey	Grey

Model estimates of flow duration may also be made for the Madeira Channel flows (Fig. 4C), since the total mass of sediment transported by individual flows can be approximated from their deposits. Based on extensive seafloor coring, beds 5, 7 and 12 are estimated to have volumes, V_b , within the Madeira Abyssal Plain of 30, 110 and 190 km³, respectively (Stevenson *et al.*, 2013). The sediment volume transported by each flow into the basin via the Madeira Channels is given by, $V_s = V_b c_m$, where V_s is the total transported sediment volume, V_b the bed volume and assuming a packing concentration, $c_m = 0.6$ (Dorrell & Hogg, 2010). The flow duration is given by, $T = V_s / Q_s$, where the sediment flux, $Q_s = cua$, was computed assuming a range of flow depths and depth-averaged flow velocities, applying equilibrium values of ch for $S = 10^{-3}$ (Fig. 4B). The area of the flow, a , was estimated by integrating the flow depth above the bathymetric profile. Here it is assumed that currents with heights greater than the channel depth would have spread laterally to the confining basin margins (see Appendix A5). Evidence that flows were not confined to a single channel comes from sediment cores indicating that individual flow events, including those that deposited beds 5 and 12, utilized both northern and southern channels located 40 to 50 km apart (Stevenson *et al.*, 2013; Fig. A2). Alternatively, assuming flows were narrower than the full basin width would increase the predicted flow duration. The depth-averaged flow velocity for equilibrium conditions, calculated for each model, using Eq. 8, is also plotted (Fig. 4C). Again, flows are assumed to have a median particle size, $\phi = 5$, and standard deviation, $\sigma = 1.26$, based on the average bulk values for beds in the Madeira

Abyssal Plain. Analysis for the Rouse, Cantero and Parker models, that do not solve $S = 10^{-3}$ in the limits of c and h considered appropriate for natural flows, are omitted. Based on this analysis it may be seen that the flow-power flux-balance model predicts flow durations of one to ten days at the equilibrium velocity of 2.8 m s⁻¹ (comparable to depth-averaged flow velocities within the Congo submarine channel (Vangriesheim *et al.*, 2009)). In comparison, all other models considered predict relatively low equilibrium velocities (0.18–0.54 m s⁻¹) which correspond to unrealistically long flow durations >10² days (Fig. 4C).

DISCUSSION

Summary of model comparison and controls on equilibrium

In the presented analysis, a number of different models have been evaluated using observational data for turbidity currents. A summary of the performance of models is provided in Table 2. The results show that the flow-power flux-balance model provides predictions that better fit observational data compared with the other models examined. Whilst some other models provide predictions for Shields numbers and slopes compatible with observational data, predicted flow durations are far in excess of those known for natural turbidity currents, whose longest recorded durations are 10 to 14 days (Talling *et al.*, 2013; Azpiroz-Zabala *et al.*, 2017).

As for dilute open channel flows (Dorrell *et al.*, 2018), the success of the flow-power flux-balance model is ascribed to its ability to account

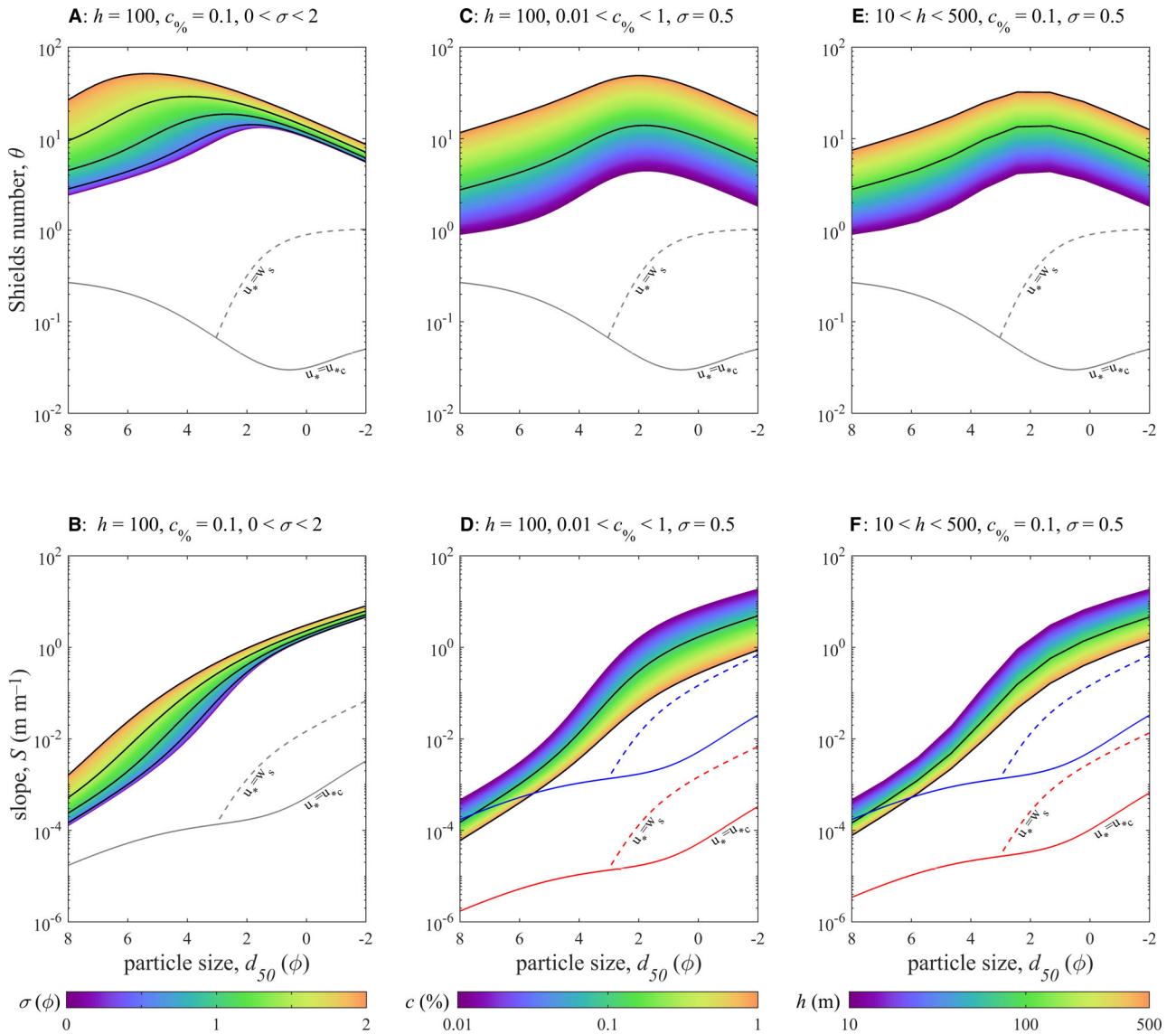


Fig. 5. Flow-power flux-balance model predicted equilibrium Shields number and equilibrium slope versus median particle diameter for variable particle size standard deviation, σ (A & B), concentration, c [%] (C & D) and flow depth, h (E & F). The threshold for motion, $u_* = u_{*c}$, and suspension, $u_* = w_s$, are shown by solid and dashed lines, respectively, noting minimum and maximum values for the former are shown in (D) and (F).

for both flow capacity and competence limits on sediment transport. Also, critically it explicitly takes into account particle size distribution, fundamental to controlling the amount of material in suspension in shear flows (McLean, 1992; Dorrell *et al.*, 2013). Model results using the flow-power flux-balance model illustrate the sensitivity of equilibrium Shields number and slope to the standard deviation of the particle size distribution, σ , flow concentration, c , and depth, h (Fig. 5). (Here and for subsequent presented results of the flow-power flux-balance model, particle size distribution is

specified in the model *a priori* by a log-normal distribution discretized into N size classes with a phi-scale bin size of 0.01, truncated to the central 99% region of the probability function to avoid overly small and large particles in the analysis.) The parameters σ , c and h impose an order of magnitude variation on equilibrium Shields number comparable or larger than the variation caused by median grain size over $-2 < \phi < 8$. The magnitude of equilibrium slope is proportionally related to particle size distribution but inversely related to flow concentration and depth. When varied

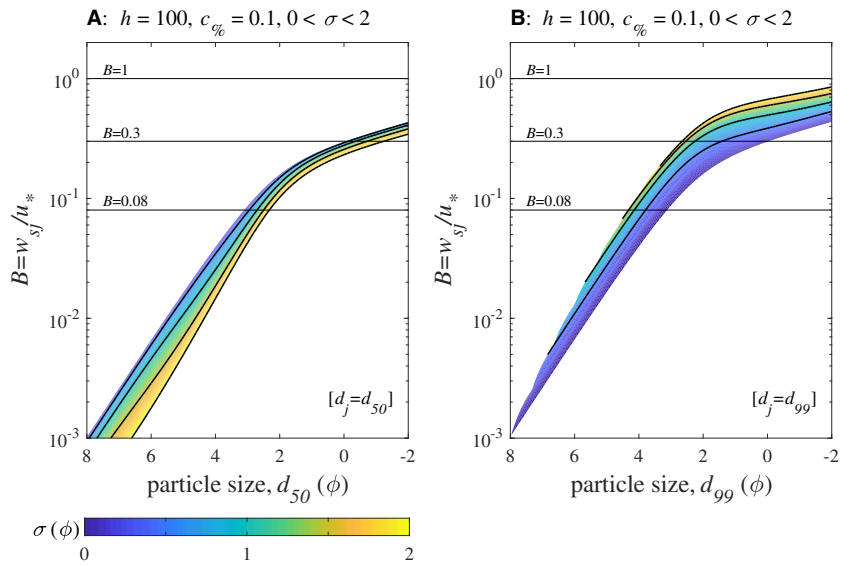


Fig. 6. Flow-power flux-balance model predicted equilibrium values for the ratio of characteristic particle settling velocity to shear velocity, B , versus characteristic particle diameter and particle size standard deviation for $d_j = d_{50}$ (A) and $d_j = d_{99}$ (B).

individually these parameters have a relatively modest impact on the equilibrium slope (Fig. 5). However, when varied together predicted slopes vary by as much as three-orders of magnitude for the same value of d_{50} (Fig. 4A).

The analysis suggests that the Rouse criterion for suspension, previously used as a criterion for the deposition of erosional–depositional thresholds (Komar, 1985; Mulder *et al.*, 1997; Kneller, 2003), substantially under-predicts equilibrium Shields numbers and slopes. Here the characteristic settling velocity, w_{sj} , used for the Rouse criterion (and other monodisperse models) is defined by the median particle size. As discussed previously, there is uncertainty as to the best grain size percentile, if one exists, to use for monodisperse models. Given the under-prediction of equilibrium shear stresses using d_{50} , application of a percentile that corresponds to a higher settling velocity should provide results with a closer agreement with observational data. However, examination of the flow-power flux-balance model suggests that equilibrium may not be predicted by a constant ratio, $B = w_{sj}/u_*$, based on a single representative particle size, including those approximating the maximum particle size such as the d_{99} (Fig. 6). Hence, these results agree with previous assessments of the Rouse criterion being an inadequate measure of suspension dynamics (Hiscott, 1994; Leeder *et al.*, 2005; Dorrell *et al.*, 2018).

Sediment transport regimes

Regimes of sediment transport are classically defined by: (i) the Shields criterion for initial

motion, θ_{ci} , above which the i^{th} particle class will begin to move as bedload; and (ii) the Rouse (or Rouse-Bagnold) criterion, θ_{si} , for suspension above which dilute particle suspensions will dominantly be transported by turbulence with limited contact with the bed. These criteria allow the distinction of four sediment transport fields: (i) no sediment transport; (ii) bedload motion; (iii) bedload and suspended load; and (iv) suspended load alone where suspended sediment is already in the flow but may not be entrained from the bed (Fig. 7A) (e.g. Leeder *et al.*, 2005, and references therein). For turbidity currents the Rouse criterion has been applied as an equilibrium criterion and taken to indicate the depositional–erosional (e.g. Komar, 1985; Mulder *et al.*, 1997; Kneller, 2003); noting a similar application for open channel flows (e.g. Lynds *et al.*, 2014). As highlighted above, the Rouse criterion is not a robust measure of equilibrium conditions for turbidity currents, agreeing with previous work for open channels (Dorrell *et al.*, 2018). The flow-power flux-balance model implies a markedly different equilibrium relationship in modified Shields space ($\theta = f(\phi)$) with substantially higher shear stresses compared to the Rouse criterion (Fig. 7B). Moreover, it indicates that equilibrium, for any single median grain size, is non-unique, i.e. flows of the same median grain size with different c , h or σ require different shear stresses for equilibrium (Fig. 5).

Considering the regimes of bedload-dominated and suspended-load-dominated sediment transport (Fig. 7A) and erosional and depositional flow regimes (Fig. 7B), four sediment transport

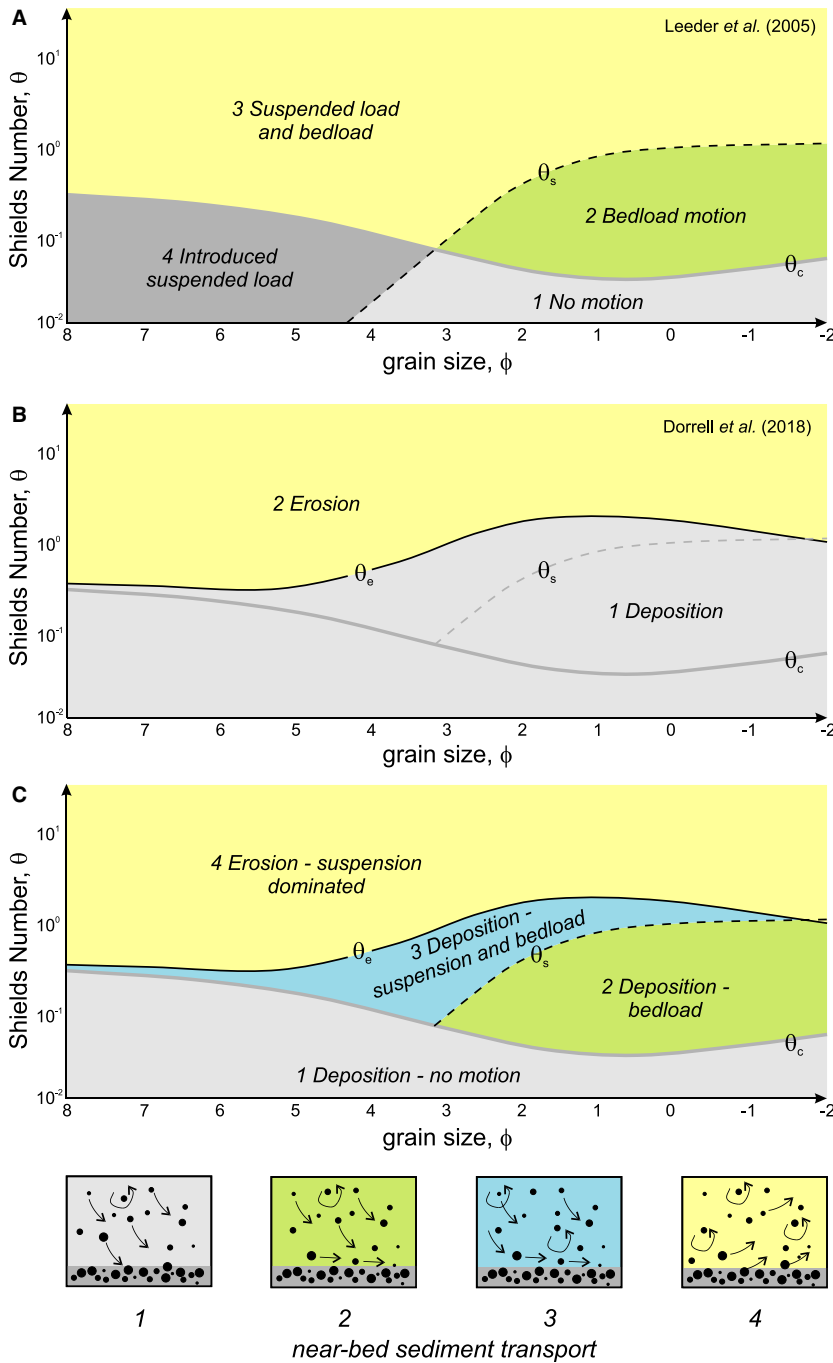
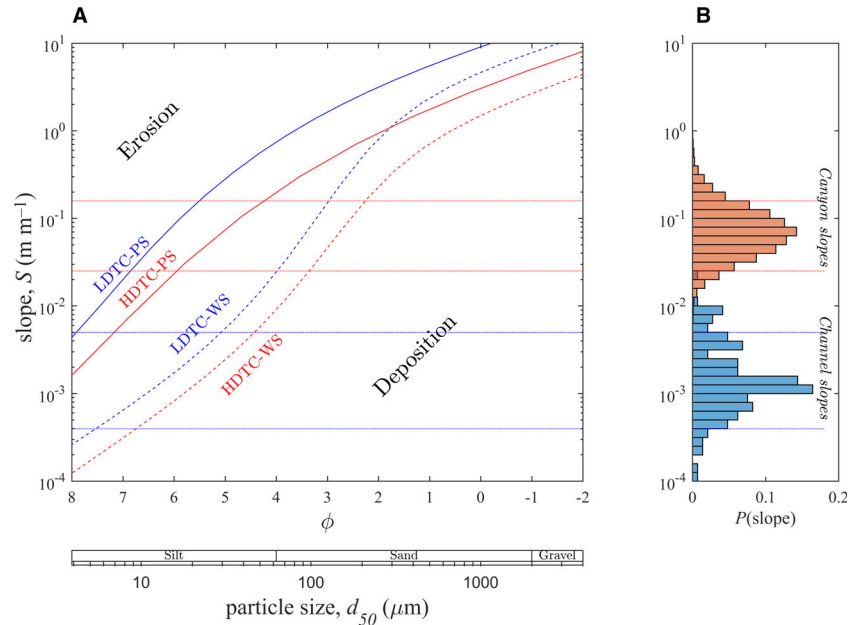


Fig. 7. Shields plots showing proposed sediment transport regimes. (A) Regimes of no motion, bedload dominated transport, suspended load dominated transport and introduced suspended load as defined by the Shields (θ_c) and Rouse (θ_s) criteria (after Leeder *et al.*, 2005). (B) Regimes of erosion and deposition as defined by the equilibrium criterion (θ_e). (C) Regimes defined by the θ_c , θ_s and θ_e criteria. Illustrations beneath show proposed near-bed sediment transport regimes in (C).

regimes may be defined assuming disequilibrium conditions: (1) deposition with direct particle fallout and no traction as bedload; (2) deposition with traction as bedload before final deposition; (3) deposition with the possibility of transitory resuspension before final deposition; and (4) erosion under suspension-dominated transport (Fig. 7C). This four-fold regime division is comparable to the scheme proposed by Halsey *et al.* (2017). Regimes 1 and 2 equate to

the ‘direct fall-out dominated’ and ‘traction-dominated’ flow boundary zones proposed by Branney & Kokelaar (2002) for ‘fully dilute’ particle-laden density currents. Regime 3 could involve transitory resuspension or unsteady deposition (Halsey *et al.*, 2017). This may occur for instance in the form of pulsatory deposition with periods of erosion, as for instance associated with ‘laminar sheared layers’ (Sumner *et al.*, 2008). Depositional regimes will be highly

Fig. 8. Flow-power flux-balance model results for equilibrium slope versus median grain size for low concentration, thick flows (LDTC) where $c = 0.01\%$ and $h = 200$ m and high concentration, shallow flows (HDTC) where $c = 1\%$ and $h = 10$ m, for well-sorted (WS) $\sigma = 0.01$ and poorly sorted (PS) $\sigma = 2$ sediment loads. Probability distribution of slopes for submarine canyons and channels based on data reported by Harris & Whiteway (2011) and Konsoer *et al.* (2013), respectively. Dashed horizontal lines show the 10th and 90th percentile values for canyon and channel slopes.



dependent on the suspended load fall-out rate (Lowe, 1988; Arnott & Hand, 1989). Under high fallout rate conditions in any of the depositional regimes 1 to 3, relatively high concentration 'granular' or 'fluid-escape' dominated flow boundary zones may develop, during which bedload traction *sensu stricto* would not operate (Branney & Kokelaar, 2002).

Critical slope for erosion/deposition

Equilibrium conditions dictate the sediment transport behaviour of flows on slopes (deposition versus erosion) and in turn the long-term evolution of the slope profile and resulting stratigraphic architecture (Kneller, 2003; Prather, 2003). The flow-power flux-balance model highlights the wide range of equilibrium slope, that marks the threshold for erosion or deposition, that may arise from realistic ranges in flow and particle parameters of turbidity currents (Figs 4A and 5). This is consistent with the observed three-order variation in slope of submarine channel systems, that are inferred to be in equilibrium with their formative flow events, and the difficulty in normalising slope for these systems with respect to bankfull channel characteristics (Konsoer *et al.*, 2013).

Figure 8 shows model results for equilibrium slopes versus median grain size for relatively: (i) thin and concentrated; and (ii) thick and dilute flows and for cases of well-sorted and poorly sorted sediment loads. Also shown in Fig. 8 are canyon and channel slopes of modern systems

(Harris & Whiteway, 2011; Konsoer *et al.*, 2013). These results illustrate the limits on erosional regimes in slope systems, noting that for erosion to occur the bed slope is required to be higher than that for equilibrium. For most canyon systems, only currents carrying suspended material with $d_{50} < ca\ 200\ \mu m$, or for slope channels material with $d_{50} < ca\ 50\ \mu m$, are predicted to be erosional; currents carrying sediment with a coarser median particle size are predicted to be depositional (Fig. 8). Even exceptionally thick and highly concentrated flows carrying well-sorted sediment, require sediment to have median grain sizes less than very coarse sand on typical canyon slopes, or fine sand on channel slopes, for erosional regimes (Fig. 4A). Alternatively, viewed from the perspective of critical slope for equilibrium, turbidity currents carrying sand grade material should commonly exhibit depositional behaviour, even on relatively steep slopes (10^{-1} – 10^0 m m⁻¹), especially if carrying poorly sorted material. This appears to be in agreement with observations of modern turbidite systems, such as the Var (Mulder *et al.*, 1997) and Monterey channel-canyon systems (Paull *et al.*, 2005; Maier *et al.*, 2019). In such small sandy systems, flows are likely to be depositional, for at least some of their duration, since channel thalwegs are covered by sand and gravel lags.

Flow evolution

Turbidity current concentration, depth and other properties, including suspended sediment

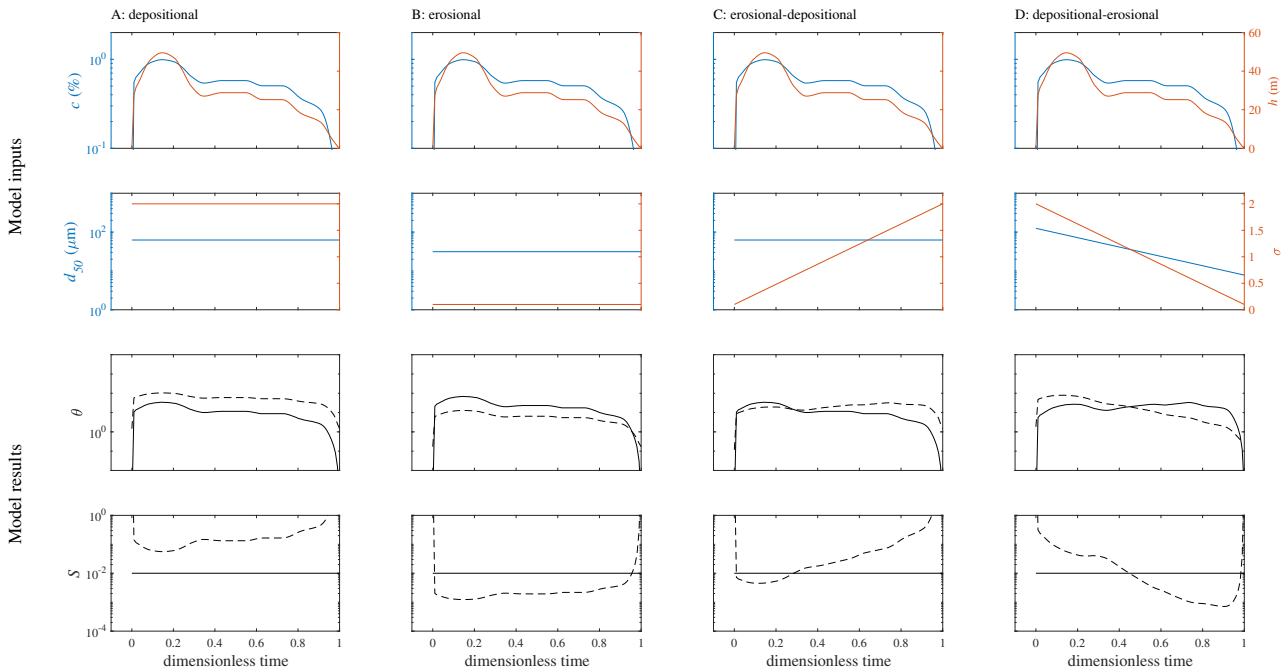


Fig. 9. Examination of temporal changes in equilibrium flow conditions using the flow-power flux-balance model, illustrating that flows may display exclusively depositional (A), erosional (B), erosional to depositional (C) or depositional to erosional (D) behaviour. Top two rows show input parameters (c [%], d , h , σ). Bottom two rows show results for equilibrium Shields stress and slope (dashed line) compared to that of the flow Shields stress and bed slope (solid line).

properties, vary spatially and temporally (Kneller, 1995; McCaffrey *et al.*, 2003). At any one location, the temporal evolution of the flow's properties will determine whether depositional or erosional regimes dominate. Flows with different temporal patterns will thus display different records of sediment transport behaviour through time. Using the flow-power flux-balance model, this may be illustrated by considering equilibrium conditions for four waning currents (Fig. 9). The hypothetical flows have the same flow properties (i.e. depth and concentration) but differ in their sediment particle size distribution. The flow shear velocity was calculated assuming a force-balance for quasi-equilibrium flow (see Appendix A3) for a specified slope ($S = 0.01$). This analysis indicates that flows can be either depositional (Fig. 9A) or erosional (Fig. 9B) throughout most of their duration; as illustrated for flows carrying relatively coarse, poorly-sorted material and fine, well-sorted material, respectively. Alternatively, under other patterns of temporal change, flows may switch from 'erosional to depositional' (Fig. 9C). This is the typically assumed mode of evolution for surge-type turbidity currents, as for

instance inferred from the Bouma sequence (Pea-kall *et al.*, 2020, and references therein), where the leading faster and more concentrated front of the current is erosional and the waning body and tail regions depositional. Finally, the opposite pattern, involving a change from depositional to erosional flow, may also occur given specific temporal variations in flow and sediment properties (Fig. 9D). This pattern of evolution has been previously inferred from turbidite beds that display internal depositional hiatuses or erosional surfaces, suggesting an initial depositional phase followed by erosion and reworking of the current's own deposit, before a final terminal depositional waning phase (Kneller & McCaffrey, 2003; Stevenson *et al.*, 2014).

CONCLUSIONS

In this paper, previously proposed equilibrium criteria for dilute turbidity currents, involving suspended-load-dominated flow of non-cohesive particles over an erodible bed, have been tested against data from laboratory experiments and

the Madeira channel system. The considered criteria include those previously described by Cantero, Halsey, Hiscott, Parker and Rouse, and a new model recently adapted for turbidity currents – the flow-power flux-balance model – based on turbulent suspension of sediment that applies a flow-power based description of sediment entrainment. It is shown that compared to other models the flow-power flux-balance model provides predictions for equilibrium Shields numbers and slopes more consistent with observational data. Notably most other models fail to predict bed slope and flow durations within limits of natural system data.

The well-known Rouse criterion for sediment suspension, $B = w_{sj}/u_*$, previously proposed as a simple proxy for equilibrium and used in palaeohydraulic estimations, is found to substantially under-predict values for equilibrium shear stress and equilibrium slope. This under-prediction may be related to the particular assumptions made in this work: the characteristic settling velocity of suspended sediment is related to the median particle size and $0.3 < B < 1$. However, results of the flow-power flux-balance model imply that B is not a constant, nor that any single characteristic particle size may be used in order to predict equilibrium. Hence, these results agree with previous assessments of the Rouse criterion being an inadequate measure of suspension dynamics lacking physical generality (Hiscott, 1994; Leeder *et al.*, 2005; Dorrell *et al.*, 2018).

Based on the model performance, it may be argued that the flow-power flux-balance model provides an improved quantification of equilibrium conditions and insights into suspension dynamics. Results from this model show the following:

- Equilibrium Shields numbers are not constant but vary substantially (by an order of magnitude) with flow and particle-size parameters, including particle size distribution, concentration and depth of flow.
- Similarly, values of equilibrium slope vary widely (by several orders of magnitude). The wide variation in slope displayed by submarine turbidite systems may be interpreted to be, at least in part, a consequence of the natural variability in flow properties and particle-sizes of transport systems.
- The erosional phase space for dilute turbidity currents is relatively restricted to those currents carrying relatively fine-grained material and on relatively steep slopes. Based on median grain size

and median slope values of modern systems, currents carrying material greater than silt or coarser would be expected to be depositional in over 50% of submarine channels, whilst those carrying fine sand or coarser should be depositional in over 50% of canyons.

- Currents should show temporal variations in sediment transport behaviour, including an evolution from depositional to erosional flow due to changes in flow and particle size distribution (as inferred previously from the depositional record).
- The flow-power flux-balance model implies a markedly different phase diagram for sediment transport regimes of dilute suspended-load dominated flows compared to that based on the classical Rouse suspension criterion.

ACKNOWLEDGEMENTS

This work was supported by the Turbidites Research Group (University of Leeds, UK) under the auspices of the 2017–2019 phase sponsored by AkerBP, Anadarko (now Oxy), BP, ConocoPhillips, ENI, HESS, Murphy, OMV and Shell. RMD would like to thank the Natural Environment Research Council for funding via the NERC Grant NE/S014535/1. We are grateful for the constructive and thorough reviews from Ben Kneller, Maarten Felix and an anonymous reviewer and the editorial oversight provided by Jaco Baas and Ian Kane.

NOTATIONS

β	Rouse number
θ	Shields number
κ	von Kármán constant
ν	Kinematic viscosity
ρ	Ambient and interstitial fluid density
ρ_s	Particle density
ρ_c	Turbidity current density
$\Delta\rho$	Difference in particle and fluid density, $\rho_s - \rho$
σ	Particle size distribution standard deviation
τ_*	Bed shear stress
ϕ	Particle size in phi units
\forall	Assertions holds for all instances
a	Flow area
C_d	Drag coefficient
c	Depth-averaged volumetric flow concentration

$c(z)$	Volumetric flow concentration at height z above the bed
c_m	Volumetric packing concentration of the bed
c^+	Volumetric concentration of suspended sediment at reference height z^+ above the bed
c^-	Volumetric concentration in the active layer at the top of the bed
d	Particle diameter
d_{50}	Median particle diameter
D_s	Dimensionless particle diameter
E_w	Ambient fluid entrainment coefficient
E_s	Dimensionless entrainment function
g	Gravitational acceleration
g'	Reduced gravity of turbidity current
h	Flow depth
K	Eddy diffusivity
L	Flow mixing length scale
N	Number of particle classes
Q_s	Sediment flux
R	Submerged specific density of a particle
Re	Reynolds number
Re_p	Particle Reynolds number
Ri	Bulk Richardson number
S	Slope (m/m)
T	Flow duration
u	Depth-averaged flow velocity
$u(z)$	Flow velocity at height z above the bed
u^*	Shear velocity
V_b	Bed volume
V_s	Sediment volume
w_s	Particle settling velocity
z	Height above the bed
z^+	Reference height above the bed
Z	Dimensionless height above the bed
Z^+	Dimensionless reference height above the bed

Subscripts

\cdot_i	Index parameter indicating the i th particle class
\cdot_j	Value for the characteristic particle diameter, here taken as d_{50} unless otherwise stated
\cdot_N	Value for $i=N$ particle class i.e. largest particle class i.e. largest particle class
\cdot_c	Critical value for incipient motion

DATA AVAILABILITY STATEMENT

The data that support the findings of this study are available from the corresponding author upon reasonable request.

REFERENCES

- Abad, J.D., Sequeiros, O.E., Spinewine, B., Pirmez, C., Garcia, M.H. and Parker, G. (2011) Secondary Current of Saline Underflow In A Highly Meandering Channel: Experiments and Theory. *J. Sediment. Res.*, **81**, 787–813. <https://doi.org/10.2110/jsr.2011.61>
- Amy, L.A. (2019) A review of producing fields inferred to have upslope stratigraphically trapped turbidite reservoirs: Trapping styles (pure and combined), pinch-out formation, and depositional setting. *AAPG Bulletin*, **103**(12), 2861–2889. <https://doi.org/10.1306/02251917408>
- Amy, L.A. and Dorrell, R.D. (2021) Equilibrium sediment transport, grade and discharge for suspended-load-dominated flows on Earth, Mars and Titan. *Icarus*, **360**, 114243. <https://doi.org/10.1016/j.icarus.2020.114243>
- Amy, L.A., Talling, P.J., Edmonds, V.O., Sumner, E.J. and Lesueur, A. (2006) An experimental investigation of sand–mud suspension settling behaviour: implications for bimodal mud contents of submarine flow deposits. *Sedimentology*, **53**, 1411–1434. <https://doi.org/10.1111/j.1365-3091.2006.00815.x>
- Arnott, R.W.C. and Hand, B.M. (1989) Bedforms, Primary Structures and Grain Fabric in the Presence of Suspended Sediment Rain. *SEPM J. Sediment. Res.*, **59**, 1062–1069. <https://doi.org/10.1306/212f90f2-2b24-11d7-8648000102c1865d>
- Azpiroz-Zabala, M., Cartigny, M.J.B., Talling, P.J., Parsons, D.R., Sumner, E.J., Clare, M.A., Simmons, S.M., Cooper, C. and Pope, E.L. (2017) Newly recognized turbidity current structure can explain prolonged flushing of submarine canyons. *Science Advances*, **3**, e1700200. <https://doi.org/10.1126/sciadv.1700200>
- Baas, J.H., Best, J.L., Peakall, J. and Wang, M. (2009) A Phase Diagram for Turbulent, Transitional, and Laminar Clay Suspension Flows. *J. Sediment. Res.*, **79**(3–4), 162–183. <https://doi.org/10.2110/jsr.2009.025>
- Bagnold, R.A. (1966) *An Approach to the Sediment Transport Problem from General Physics*, Vol. **442-I**. U.S. Geological Survey Professional Paper, Washington, DC.
- Bell, H.S. (1942) Studies for Students: Density Currents as Agents for Transporting Sediments. *J. Geol.*, **50**, 512–547. <https://doi.org/10.1086/625070>
- Bennett, S.J., Bridge, J.S. and Best, J.L. (1998) Fluid and sediment dynamics of upper stage plane beds. *J. Geophys. Res. Oceans*, **103**(C1), 1239–1274. <https://doi.org/10.1029/97jc02764>
- Branney, M.J. and Kokelaar, B.P. (2002) Pyroclastic Density Currents and the Sedimentation of Ignimbrites. Geological Society of London Memoir 27. London: Geological Society of London, 2002. 143 pages. *J. Geol.*, **113**, 115–116. <https://doi.org/10.1086/427850>
- Buckee, C., Kneller, B. and Peakall, J. (2001) Turbulence structure in steady, solute-driven gravity currents. In: *Particulate Gravity Currents, Special Publication 31 of the International Association of Sedimentologists* (Eds

- McCaffrey, W. D., Kneller, B. C. and Peakall, J.), Vol. 31. Blackwell Science, Oxford.
- Burr, D., Emery, J., Lorenz, R., Collins, G. and Carling, P.** (2006) Sediment transport by liquid surficial flow: Application to Titan. *Icarus*, **181**, 235–242. <https://doi.org/10.1016/j.icarus.2005.11.012>
- Buscall, R.** (1990) The sedimentation of concentrated colloidal suspensions. *Colloids Surfaces*, **43**, 33–53. [https://doi.org/10.1016/0166-6622\(90\)80002-L](https://doi.org/10.1016/0166-6622(90)80002-L)
- Camenen, B. and Larson, M.** (2008) A general formula for noncohesive suspended sediment transport. *J. Coastal Res.*, **24**(3), 615–627.
- Cantero, M.I., Shringarpure, M. and Balachandar, S.** (2012) Towards a universal criteria for turbulence suppression in dilute turbidity currents with non-cohesive sediments. *Geophys. Res. Lett.*, **39**, <https://doi.org/10.1029/2012gl052514>
- Caulfield, C.P.** (2021) Layering, Instabilities, and Mixing in Turbulent Stratified Flows. *Annu. Rev. Fluid Mech.*, **53**, 113–145. <https://doi.org/10.1146/annurev-fluid-042320-100458>
- Cellino, M. and Graf, W.H.** (1999). Sediment-Laden Flow in Open-Channels under Noncapacity and Capacity Conditions. *J. Hydraulic Eng.*, **125**(455), 455–462. [https://doi.org/10.1061/\(ASCE\)0733-9429\(1999\)125](https://doi.org/10.1061/(ASCE)0733-9429(1999)125)
- Clare, M.D., Lintern, G., Rosenberger, K., Hughes Clarke, J.E., Paull, C., Gwiazda, R., Cartigny, M.J.B., Talling, P.J., Perara, D., Xu, J., Parsons, D., Silva, J.R. and Apprioual, R.** (2020) Lessons learned from the monitoring of turbidity currents and guidance for future platform designs. *Geol. Soc., London, Spec. Public.*, **500**(1), 605–634. <https://doi.org/10.1144/SP500-2019-173>
- Cossu, R. and Wells, M.** (2012) A comparison of the shear stress distribution in the bottom boundary layer of experimental density and turbidity currents. *Eur. J. Mech. B/Fluids*, **32**, 70–79. <https://doi.org/10.1016/j.euromechflu.2011.09.006>
- Crisóstomo-Figueroa, A., McArthur, A.D., Dorrell, R.M., Amy, L.A. and McCaffrey, W.D.** (2020) A new modelling approach to sediment bypass prediction applied to the East Coast Basin, New Zealand. *GSA Bulletin*, **133**(7–8), 1734–1748. <https://doi.org/10.1130/B35687.1>
- Dade, W.B. and Friend, P.F.** (1988) Grain-size, sediment-Transport Regime, and channel slope in alluvial rivers. *J. Geol.*, **106**, 661–676. <https://doi.org/10.1086/516052>
- Davies, R.** (1968) The experimental study of the differential settling of particles in suspension at high concentrations. *Powder Technol.*, **2**, 43–51. [https://doi.org/10.1016/0032-5910\(68\)80032-4](https://doi.org/10.1016/0032-5910(68)80032-4)
- Dorrell, R., Amy, L.A., Peakall, J. and McCaffrey, W.D.** (2018) Particle-size distribution controls the threshold between net sediment erosion and deposition in suspended load dominated flows. *Geophys. Res. Lett.*, **45**, 1443–1452. <https://doi.org/10.1002/2017GL076489>
- Dorrell, R.M., Burns, A.D. and McCaffrey, W.D.** (2015) The inherent instability of leveed seafloor channels. *Geophys. Res. Lett.*, **42**(10), 4023–4031. <https://doi.org/10.1002/2015GL063809>
- Dorrell, R. and Hogg, A.J.** (2010) Sedimentation of bidisperse suspensions. *Int. J. Multiph. Flow*, **36**, 481–490. <https://doi.org/10.1016/j.ijmultiphaseflow.2010.02.001>
- Dorrell, R.M. and Hogg, A.J.** (2012) Length and time scales of response of sediment suspensions to changing flow conditions. *J. Hydraulic Eng.*, **138**, 430–439. [https://doi.org/10.1061/\(ASCE\)HY.1943-7900.0000532](https://doi.org/10.1061/(ASCE)HY.1943-7900.0000532)
- Dorrell, R.M., Hogg, A.J. and Pritchard, D.** (2013) Polydisperse suspensions: Erosion, deposition, and flow capacity. *J. Geophys. Res.*, **118**, 1939–1955. <https://doi.org/10.1002/jgrf.20129>
- Dorrell, R.M., Peakall, J., Darby, S.E., Parsons, D.R., Johnson, J., Sumer, E.J., Wynn, R.B., Özsoy, E. and Tezcan, D.** (2019) Self-sharpening induces jet-like structure in seafloor gravity currents. *Nat. Commun.*, **10**, 1381. <https://doi.org/10.1038/s41467-019-09254-2>
- Eggenhuisen, J.T., Tilston, M.C., Leeuw, J., Pohl, F. and Cartigny, M.J.** (2019) Turbulent diffusion modelling of sediment in turbidity currents: An experimental validation of the Rouse approach. *Depos. Rec.*, **6**(1), 203–216. <https://doi.org/10.1002/dep2.86>
- Einstein, H.** (1950) *Transport of Sediment Mixtures with Large Ranges of Grain Sizes*. Dept. of Agriculture, US, Washington, DC.
- Elghobashi, S.** (1994) On predicting particle-laden turbulent flows. *Appl. Sci. Res.*, **52**, 309–329. <https://doi.org/10.1007/BF00936835>
- Galy, V., France-Lanord, C., Beyssac, O., Faure, P., Kudrass, H. and Palhol, F.** (2007) Efficient organic carbon burial in the Bengal fan sustained by the Himalayan erosional system. *Nature*, **450**, 407–410. <https://doi.org/10.1038/nature06273>
- Garcia, M.H.** (2008) Sediment transport and morphodynamics. In: *Sedimentation engineering: Processes, measurements, modeling and practice*. ASCE manuals and reports on engineering practice No. 110 (Ed. Garcia, M.H.), pp. 21–164. American Society of Civil Engineers, Reston, VA. <https://doi.org/10.1061/9780784408148.ch02>
- Garcia, M.H. and Parker, G.** (1991) Entrainment of bed sediment into suspension. *J. Hydraul. Eng.*, **117**(4), 414–435. [https://doi.org/10.1061/\(ASCE\)0733-9429\(1991\)117:4\(414\)](https://doi.org/10.1061/(ASCE)0733-9429(1991)117:4(414))
- Garcia, M.H. and Parker, G.** (1993) Experiments on the entrainment of sediment into suspension by a dense bottom current. *J. Geophys. Res.*, **98**(C3), 4793–4807. <https://doi.org/10.1029/92JC02404>
- Gray, T.E., Alexander, J. and Leeder, M.R.** (2005) Quantifying velocity and turbulence structure in depositing sustained turbidity currents across breaks in slope. *Sedimentology*, **52**, 467–488. <https://doi.org/10.1111/j.1365-3091.2005.00705.x>
- Gray, T.E., Alexander, J. and Leeder, M.R.** (2006) Longitudinal flow evolution and turbulence structure of dynamically similar, sustained, saline density and turbidity currents. *J. Geophys. Res.*, **111**, <https://doi.org/10.1029/2005jc003089>
- Halsey, T.C., Kumar, A. and Perillo, M.M.** (2017) Sedimentological regimes for turbidity currents depth-averaged theory. *J. Geophys. Res. Oceans*, **122**, 5260–5285. <https://doi.org/10.1002/2016JC012635>
- Harris, T.H. and Whiteway, T.** (2011) Global distribution of large submarine canyons: Geomorphic differences between active and passive continental margins. *Mar. Geol.*, **285**, 69–86. <https://doi.org/10.1016/j.margeo.2011.05.008>
- Hirano, M.** (1971) River bed degradation with armoring [in Japanese]. *Proc. Jpn. Soc. Civil Eng.*, **195**, 55–65. https://doi.org/10.2208/jscej1969.1971.195_55
- Hiscott, R.N.** (1994) Loss of capacity, not competence, as the fundamental process governing deposition from turbidity currents. *J. Sediment. Res.*, **A64**, 209–214. <https://doi.org/10.2110/jsr.64.209>
- Janocko, M., Cartigny, M.B.J., Nemec, W. and Hansen, E.W.M.** (2013) Turbidity current hydraulics and sediment deposition in erodible sinuous channels: Laboratory

- experiments and numerical simulations. *Mar. Pet. Geol.*, **41**, 222–249. <https://doi.org/10.1016/j.marpetgeo.2012.08.012>
- Kane, I.A.** and **Clare, M.** (2019) Dispersion, accumulation and the ultimate fate of microplastics in deep-marine environments: a review and future directions. *Front. Earth Sci.*, **7**, 80. <https://doi.org/10.3389/feart.2019.00080>
- Kneller, B.** (1995) Beyond the turbidite paradigm: physical models for deposition of turbidites and their implications for reservoir prediction. *Geol. Soc., London, Spec. Public.*, **94**, 31–49. <https://doi.org/10.1144/gsl.sp.1995.094.01.04>
- Kneller, B.** (2003) The influence of flow parameters on turbidite slope channel architecture. *Mar. Pet. Geol.*, **20**(6–8), 901–910. <https://doi.org/10.1016/j.marpetgeo.2003.03.001>
- Kneller, B.** and **Buckee, C.** (2000) The structure and fluid mechanics of turbidity currents: a review of some recent studies and their geological implications. *Sedimentology*, **47**, 62–94. <https://doi.org/10.1046/j.1365-3091.2000.047s1062.x>
- Kneller, B.C.** and **McCaffrey, W.D.** (2003) The Interpretation of Vertical Sequences in Turbidite Beds: The Influence of Longitudinal Flow Structure. *J. Sediment. Res.*, **73**, 706–713. <https://doi.org/10.1306/031103730706>
- Kneller, B., Nasr-Azadani, M.M., Radhakrishnan, S.** and **Meiburg, E.** (2016) Long-range sediment transport in the world's oceans by stably stratified turbidity currents. *J. Geophys. Res. Oceans*, **121**, 8608–8620. <https://doi.org/10.1002/2016JC011978>
- Komar, P.D.** (1980) Modes of sediment transport in channelized water flows with ramifications to the erosion of the Martian outflow channels. *Icarus*, **42**, 317–329. [https://doi.org/10.1016/0019-1035\(80\)90097-4](https://doi.org/10.1016/0019-1035(80)90097-4)
- Komar, P.D.** (1985) The hydraulic interpretation of turbidites from their grain sizes and sedimentary structures. *Sedimentology*, **32**, 395–407. <https://doi.org/10.1111/j.1365-3091.1985.tb00519.x>
- Konsoer, K., Zinger, J.** and **Parker, G.** (2013) Bankfull hydraulic geometry of submarine channels created by turbidity currents: Relations between bankfull channel characteristics and formative flow discharge. *J. Geophys. Res., Series F*, **118**, 216–228. <https://doi.org/10.1029/2012jf002422>
- Kranenburg, C.** (1994) The fractal structure of cohesive sediment aggregates. *Estuar. Coast. Shelf Sci.*, **39**, 451–460. [https://doi.org/10.1016/S0272-7714\(06\)80002-8](https://doi.org/10.1016/S0272-7714(06)80002-8)
- Krumbein, W.C.** (1934) Size frequency distributions of sediments. *J. Sediment. Petrol.*, **4**, 65–77. <https://doi.org/10.1306/D4268EB9-2B26-11D7-8648000102C1865D>
- Kubo, Y.** (2004) Experimental and numerical study of topographic effects on deposition from two-dimensional, particle-driven density currents. *Sed. Geol.*, **164**, 311–326. <https://doi.org/10.1016/j.sedgeo.2003.11.002>
- Kubo, Y., Syvitski, J.P., Hutton, E.W.** and **Paola, C.** (2005) Advance and application of the stratigraphic simulation model 2D-SedFlux: From tank experiment to geological scale simulation. *Sed. Geol.*, **178**, 187–195. <https://doi.org/10.1016/j.sedgeo.2005.04.005>
- Kuenen, P.** (1937) Experiments in connection with Daly's hypothesis on the formation of submarine canyons. *Leidse Geol. Meded.*, **7**, 327–351.
- Kuenen, P.H.** and **Sengupta, S.** (1970) Experimental marine suspension currents, competence and capacity. *Geol. Mijnbouw*, **49**, 89–118.
- Leeder, M.R., Gray, T.E.** and **Alexander, J.** (2005) Sediment suspension dynamics and a new criterion for the maintenance of turbulent suspensions. *Sedimentology*, **52**, 683–691. <https://doi.org/10.1111/j.1365-3091.2005.00720.x>
- de Leeuw, J.D., Eggenhuisen, J.T.** and **Cartigny, M.J.B.** (2018) Linking submarine channel-levee facies and architecture to flow structure of turbidity currents: insights from flume tank experiments. *Sedimentology*, **65**, 931–951. <https://doi.org/10.1111/sed.12411>
- de Leeuw, J., Lamb, M.P., Parker, G., Moodie, A.J., Haught, D., Venditti, J.G.** and **Nittrouer, J.A.** (2020) Entrainment and suspension of sand and gravel. *Earth Surface Dynamics*, **8**(2), 485–504. <https://doi.org/10.5194/esurf-8-485-2020>
- Lowe, D.R.** (1988) Suspended-load fallout rate as an independent variable in the analysis of current structures. *Sedimentology*, **35**, 765–776. <https://doi.org/10.1111/j.1365-3091.1988.tb01250.x>
- Lynds, R.M., Mohrig, D., Hajek, E.A.** and **Heller, P.L.** (2014) Paleoslope reconstruction in sandy suspended-load dominated rivers. *J. Sediment. Res.*, **84**(10), 825–836. <https://doi.org/10.2110/jsr.2014.60>
- Maier, K.L., Gales, J.A., Paull, C.K., Rosenberger, K., Talling, P.J., Simmons, S.M., Gwiadzda, R., McGann, M., Cartigny, M.J.B., Lundsten, E., Anderson, K., Clare, M.A., Xu, J., Parsons, D., Barry, J.P., Wolfson-Schwehr, M., Nieminski, N.M.** and **Sumner, E.J.** (2019) Linking Direct Measurements of Turbidity Currents to Submarine Canyon-Floor Deposits. *Front. Earth Sci.*, **7**, 144. <https://doi.org/10.3389/feart.2019.00144>
- McCaffrey, W., Choux, C., Baas, J.** and **Haughton, P.** (2003) Spatio-temporal evolution of velocity structure, concentration and grain-size stratification within experimental particulate gravity currents. *Mar. Pet. Geol.*, **20**, 851–860. <https://doi.org/10.1016/j.marpetgeo.2003.02.002>
- McLean, S.R.** (1992) On the calculation of suspended load for noncohesive sediments. *J. Geophys. Res.*, **97**, 5759. <https://doi.org/10.1029/91jc02933>
- Meiburg, E.** and **Kneller, B.** (2010) Turbidity currents and their deposits. *Ann. Rev. Fluid Mech.*, **42**, 135–156. <https://doi.org/10.1146/annurev-fluid-121108-145618>
- Meiburg, E., Nasr-Azadani, M.** and **Radhakrishnan, A.** (2015) Modeling Gravity and Turbidity Currents: Computational Approaches and Challenges. *Appl. Mech. Rev.*, **67**, 40802. <https://doi.org/10.1115/1.4031040>
- Middleton, G.V.** and **Hampton, M.A.** (1973) Sediment gravity flows: mechanics of flow and deposition. In: *Turbidites and Deep-Water Sedimentation* (Eds Middleton, G.V. and Bouma, A.H.), *SEPM, Pacific Section, Short Course Lecture Notes*. Society of Economic Paleontologist and Mineralogist, Tulsa, 1–38. Available at: <https://www.worldcat.org/title/turbidites-and-deep-water-sedimentation-lecture-notes-for-a-short-coursesponsored-by-the-pacific-section-sepm-and-in-anaheim-may-12-1973/oclc/1123633765?referer=di&ht=edition>
- Mulder, T., Savoye, B.** and **Syvitski, J.P.M.** (1997) Numerical modelling of a mid-sized gravity flow: the 1979 Nice turbidity current (dynamics, processes, sediment budget and seafloor impact). *Sedimentology*, **44**, 305–326. <https://doi.org/10.1111/j.1365-3091.1997.tb01526.x>
- Niño, Y., Lopez, F.** and **Garcia, M.** (2003) Threshold for particle entrainment into suspension. *Sedimentology*, **50** (2), 247–263. <https://doi.org/10.1046/j.1365-3091.2003.00551.x>
- Pantin, H.M.** and **Franklin, M. C.** (2011) Improved experimental evidence for autosuspension. *Sed. Geol.*, **237**, 46–54. <https://doi.org/10.1016/j.sedgeo.2011.02.002>

- Parker, G.** (1982) Conditions for the ignition of catastrophically erosive turbidity currents. *Mar. Geol.*, **46**, 307–327. [https://doi.org/10.1016/0025-3227\(82\)90086-X](https://doi.org/10.1016/0025-3227(82)90086-X)
- Parker, G., Fukushima, Y. and Pantin, H.M.** (1986) Self-accelerating turbidity currents. *J. Fluid Mech.*, **171**, 145–181. <https://doi.org/10.1017/S0022112086001404>
- Parsons, A.J., Cooper, J. and Wainwright, J.** (2015) What is suspended sediment? *Earth Surf. Process. Landf.*, **40**(10), 1417–1420. <https://doi.org/10.1002/esp.3730>
- Paull, C.K., Mitts, P., Ussler, W., Keaten, R. and Greene, H.G.** (2005) Trail of sand in upper Monterey Canyon: Offshore California. *Geol. Soc. Am. Bull.*, **117**, 1134. <https://doi.org/10.1130/b25390.1>
- Peakall, J., Best, J., Baas, J.H., Hodgson, D.M., Clare, M.A., Talling, P.J., Dorrell, R.M. and Lee, D.R.** (2020) An integrated process-based model of flutes and tool marks in deep-water environments: Implications for palaeohydraulics, the Bouma sequence and hybrid event beds. *Sedimentology*, **67**(4), 1601–1666. <https://doi.org/10.1111/sed.12727>
- Peakall, J., McCaffrey, B. and Kneller, B.** (2000) A Process Model for the Evolution, Morphology, and Architecture of Sinuous Submarine Channels. *SEPM J. Sediment. Res.*, **70**, 434–448. <https://doi.org/10.1306/d4268c20-2b26-11d7-8648000102c1865d>
- Peltier, W.R. and Caulfield, C.P.** (2003) Mixing efficiency in stratified shear flows. *Annu. Rev. Fluid Mech.*, **35**(1), 135–167. <https://doi.org/10.1146/annurev.fluid.35.101101.161144>
- Pirmez, C., Beaubouef, R.T., Friedmann, S.J. and Mohrig, D.C.** (2000). Equilibrium Profile and base-level in submarine channels: examples from Late Pleistocene systems and implications for the architecture of deepwater reservoirs. In: *Deep-water Reservoirs of the World* (Eds Weimer, P., Slatt, R.M., Coleman, J., Rosen, N.C., Nelson, H., Bouma, A.H., Styzen, M.J. and Lawrence, D.T.), *SEPM Gulf Coast Section 20th Bob F. Perkins Research Conference*, 782–805.
- Pohl, F., Eggenhuisen, J.T., Kane, I.A. and Clare, M.A.** (2020a) Transport and burial of microplastics in deep-marine sediments by turbidity currents. *Environ. Sci. Technol.*, **54**, 4180–4189. <https://doi.org/10.1021/acs.est.9b07527>
- Pohl, F., Eggenhuisen, J., Cartigny, M., Tilston, M., Leeuw, J.D. and Hermidas, N.** (2020b) The influence of a slope break on turbidite deposits: An experimental investigation. *Mar. Geol.*, **424**, <https://doi.org/10.1016/j.margeo.2020.106160>
- Prather, B.E.** (2003) Controls on reservoir distribution, architecture and stratigraphic trapping in slope settings. *Mar. Pet. Geol.*, **20**, 529–545. <https://doi.org/10.1016/j.marpetgeo.2003.03.009>
- Richardson, J.F. and Zaki, W.N.** (1954) Sedimentation and fluidisation: part I. *Trans. Inst. Chem. Eng.*, **32**, 35–53.
- van Rijn, L.C.** (1984) Sediment transport, part II: suspended load transport. *J. Hydraul. Eng.*, **110**(11), 1613–1641. [https://doi.org/10.1061/\(ASCE\)0733-9429\(1984\)110:11\(1613\)](https://doi.org/10.1061/(ASCE)0733-9429(1984)110:11(1613))
- Rouse, H.** (1937) Modern conceptions of the mechanics or fluid turbulence. *Transactions of the American Society of Civil Engineers*, **102**, 463–505. <https://doi.org/10.1061/TACEAT.0004872>
- Schlünz, B. and Schneider, R.R.** (2000) Transport of terrestrial organic carbon to the oceans by rivers: re-estimating flux- and burial rates. *Int. J. Earth Sci.*, **88**, 599–606. <https://doi.org/10.1007/s005310050290>
- Sequeiros, O.E., Mosquera, R. and Pedocchi, F.** (2018) Internal Structure of a Self-Accelerating Turbidity Current. *J. Geophys. Res. Oceans*, **123**, 6260–6276. <https://doi.org/10.1029/2018jc014061>
- Sequeiros, O.E., Spinewine, B., Beaubouef, R.T., Sun, T., García, M.H. and Parker, G.** (2010) Characteristics of Velocity and Excess Density Profiles of Saline Underflows and Turbidity Currents Flowing over a Mobile Bed. *J. Hydraul. Eng.*, **136**(7), 412–433. [https://doi.org/10.1061/\(asce\)hy.1943-7900.0000200](https://doi.org/10.1061/(asce)hy.1943-7900.0000200)
- Shields, A.** (1936) *Anwendung der Aehnlichkeitsmechanik und der Turbulenzforschung auf die Geschiebepbewegung*. Preussischen Versuchsanstalt für Wasserbau, Berlin.
- Smith, J.D. and Hopkins, T.S.** (1973) Sediment transport on the continental shelf off of Washington and Oregon in light of recent current measurements. In: *Shelf Sediment Transport: Process and Patterns* (Eds Swift, D.J.P., Duane, D.B. and Pilkey, O.H.), pp. 143–179. Hutchinson and Ross, Stroudsburg, PA.
- Soulsby, R.** (1997) *Dynamics of Marine Sands: A Manual for Practical Applications*. Thomas Telford Publications, London.
- Stacey, M.W. and Bowen, A.J.** (1988) The vertical structure of density and turbidity currents: Theory and observations. *J. Geophys. Res.*, **93**, 3528–3542. <https://doi.org/10.1029/JC093iC04p03528>
- Stetten, E., Baudin, F., Reyss, J.-L., Martinez, P., Charlier, K., Schnyder, J., Rabouille, C., Dennielou, B., Coston-Guarini, J. and Pruski, A.M.** (2015) Organic matter characterization and distribution in sediments of the terminal lobes of the Congo deep-sea fan: Evidence for the direct influence of the Congo River. *Mar. Geol.*, **369**, 182–195. <https://doi.org/10.1016/j.margeo.2015.08.020>
- Stevenson, C.J., Jackson, C.-A.-L., Hodgson, D.M., Hubbard, S.M. and Eggenhuisen, J.T.** (2015) Deep-Water Sediment Bypass. *J. Sediment. Res.*, **85**, 1058–1081. <https://doi.org/10.2110/jsr.2015.63>
- Stevenson, C.J., Talling, P.J., Wynn, R.B., Masson, D.G., Hunt, J.E., Frenz, M., Akhmetzhanov, A. and Cronin, B.T.** (2013) The flows that left no trace: Very large-volume turbidity currents that bypassed sediment through submarine channels without eroding the sea floor. *Mar. Pet. Geol.*, **41**, 186–205. <https://doi.org/10.1016/j.marpetgeo.2012.02.008>
- Stevenson, C.J., Talling, P.J., Masson, D.G., Sumner, E.J., Frenz, M. and Wynn, R.B.** (2014) The spatial and temporal distribution of grain-size breaks in turbidites. *Sedimentology*, **61**, 1120–1156. <https://doi.org/10.1111/sed.12091>
- Sumner, E.J., Amy, L.A. and Talling, P.J.** (2008) Deposit Structure and Processes of Sand Deposition from Decelerating Sediment Suspensions. *J. Sediment. Res.*, **78**, 529–547. <https://doi.org/10.2110/jsr.2008.062>
- Talling, P.J., Paull, C.K. and Piper, D.J.** (2013) How are subaqueous sediment density flows triggered, what is their internal structure and how does it evolve? Direct observations from monitoring of active flows. *Earth Sci. Rev.*, **125**, 244–287. <https://doi.org/10.1016/j.earscirev.2013.07.005>
- Talling, P.J., Wynn, R.B., Masson, D.G., Frenz, M., Cronin, B.T., Schiebel, R., Akhmetzhanov, A.M., Dallmeier-Tiessen, S., Benetti, S., Weaver, P.P.E., Georgiopoulou, A., Zühlsdorff, C. and Amy, L.A.** (2007) Onset of submarine debris flow deposition far from original giant landslide. *Nature*, **450**, 541–544. <https://doi.org/10.1038/nature06313>
- Teles, V., Chauveau, B., Joseph, P., Weill, P. and Maktouf, F.** (2016) CATS – A process-based model for turbulent turbidite systems at the reservoir scale. *C.R. Geosci.*, **348**, 489–498. <https://doi.org/10.1016/j.crte.2016.03.002>

- Vangriesheim, A., Khripounoff, A. and Crassous, P. (2009) Turbidity events observed in situ along the Congo submarine channel. *Deep-Sea Res. II*, **56**, 2208–2222. <https://doi.org/10.1016/j.dsr2.2009.04.004>
- Wells, M.G. and Dorrell, R.M. (2021) Turbulence processes within turbidity currents. *Ann. Re. Fluid Mech.*, **53**, 59–83. <https://doi.org/10.1146/annurev-fluid-010719-060309>
- Zeng, J. and Lowe, D. (1997) Numerical simulation of turbidity current flow and sedimentation: I. Theory.

Sedimentology, **44**, 67–84. <https://doi.org/10.1111/j.1365-3091.1997.tb00424.x>

- Zyserman, J.A. and Fredsoe, J. (1994) Data analysis of bed concentration of suspended sediment. *J. Hydraul. Eng.*, **120**(9), 1021–1042. [https://doi.org/10.1061/\(ASCE\)0733-9429\(1994\)120:9\(1021\)](https://doi.org/10.1061/(ASCE)0733-9429(1994)120:9(1021))

Manuscript received 30 July 2020; revision 20 April 2021; revision accepted 12 July 2021

APPENDIX 1

A1 EXPERIMENTAL DATA SOURCES AND FLOW CONDITIONS

Velocity, concentration and particle size distribution data for sustained laboratory turbidity currents in straight channels were collated from six published experimental studies (Gray *et al.*, 2005, 2006; de Leeuw *et al.*, 2018; Sequeiros *et al.*, 2018; Eggenhuisen *et al.*, 2019; Pohl *et al.*, 2020b). In the following, experiments are referred to by their numbers 1–12 in Table A1 noting experiments 2 and 3 each provide measurements from two downstream locations. All experiments are ‘sustained flows’ generated by continuous pump feed systems. These studies provide information for depositional, non-depositional ‘bypassing’ and accelerative (implying erosional) turbidity currents. Experiments 5–10 were depositional over their full run-out distance and experiment 12 is described as depositional. Experiment 2 is described as being in a state of bypass and experiment 3 as self-accelerating. In the case of experiment 2, front velocities at distances >8 m downstream of the inlet were decelerative and temporal mass derivatives were negative, showing a loss of suspended sediment such that the current may be interpreted as mildly depositional. Experiment 3 displayed a continuous increase in front velocity and a positive suspended sediment mass derivative at $x = 5.5$ m, but a slightly negative sediment mass derivative further downstream ($x = 9.5$ m), indicating the suspended sediment mass tended towards equilibrium. Experiments 1 and 4 are described as completely bypassing (i.e. non-depositional) and in the latter case accelerative. Experiment 11 is described as being non-depositional. Flows in experiments 1–4 and 11–12

were run on uniform slopes. Experiments 5–10 were run on a tank floor with a change in slope, however, flow parameters used here are only from locations upstream of the slope break.

A2 EXPERIMENT BULK FLOW PARAMETERS

Depth-averaged values of flow velocity, concentration, median particle size and particle size distribution were required to calculate Shields stresses for laboratory flows and for inputs for equilibrium models. These experimental parameters are summarized in Table A1. The velocity and concentration values for each experiment are derived from measurements taken at the same horizontal location or within *ca* 20 cm of one another. Depth-averaged flow velocity, u , and concentration, c , were calculated by integration of vertical profiles:

$$uh = \int_0^h u(z) dz \quad (\text{A1})$$

$$ch = \int_0^h c(z) dz \quad (\text{A2})$$

where $u(z)$ and $c(z)$ are measured velocity and concentration at height above the bed, z , and h is the flow depth, taken to be z where $u = 0$. Note the following exceptions: (i) for experiments 2 and 3 concentration was computed from reported values of ch ; (ii) for experiments 5–10 depth-averaged flow velocity was taken from reported values; (iii) for experiment 10 concentration was computed from density profile and, due to a lack of other information, this value was taken to be representative of experiments 5–9 that had the same initial concentration.

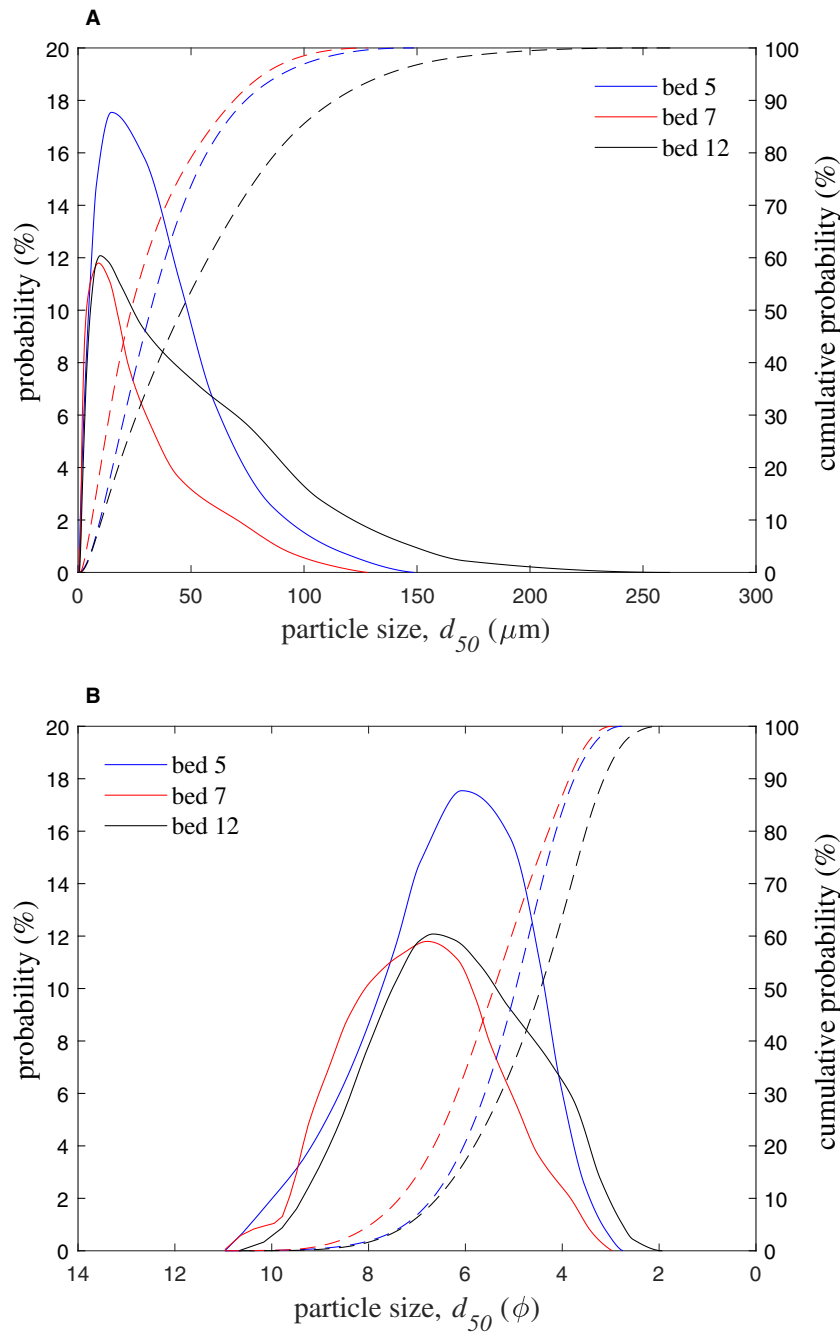


Fig. A1. Total grain-size distribution (solid) and cumulative distribution (dashed) for deposits within the Madeira Abyssal Plain shown in microns (A) and phi units (B). Based on data from Stevenson *et al.* (2014).

A3 EXPERIMENT SHEAR VELOCITY

The shear velocity for reported laboratory currents was calculated using the bulk Richardson number dependent force balance for quasi-equilibrium flow Eq. 8. Specifically, given the bulk Richardson number, $Ri = gRch/u^2$, where the submerged specific gravity of the sediment,

$R = (\rho_s/\rho) - 1$, Eq. 8 may be manipulated to provide:

$$gRchS = C_D u^2 + \frac{a}{b + Ri} \left(1 + \frac{1}{2} Ri \right) u^2 \quad (\text{A3})$$

Using $u_*^2 = C_D u^2$, Eq. A3 can be rewritten to provide the shear velocity:

Table A1. Details of experimental data for sustained laboratory turbidity currents.

Reference number	Source reference for data	Experiment name	X	S	ρ_s	ρ	h	c	u	d_{50}	σ	Ri	θ	Flow regime
			m	-	kg m ⁻³	kg m ⁻³	m	%	m s ⁻¹	ϕ	ϕ	-	-	-
1	Leeuw <i>et al.</i> (2018)	2D	2.24–2.34	0.16	2650	1000	0.12	7.31	0.40	2.77	0.86	0.89	9.31	b
2-1	Sequeiros <i>et al.</i> (2018)	Test 2	5.50	0.05	1500	1000	0.18	0.25	0.06	4.42	1.59	0.56	0.41	a
2-2	Sequeiros <i>et al.</i> (2018)	Test 2	9.50	0.05	1500	1000	0.35	0.07	0.04	4.92	2.32	0.70	0.33	d
3-1	Sequeiros <i>et al.</i> (2018)	Test 6	5.50	0.05	1500	1000	0.23	0.17	0.06	4.31	1.51	0.53	0.33	a
3-2	Sequeiros <i>et al.</i> (2018)	Test 6	9.50	0.05	1500	1000	0.23	0.26	0.07	4.56	2.16	0.62	0.64	a/b
4	Pohl <i>et al.</i> (2020b)	Bypass	2.30–2.50	0.11	2650	1000	0.11	7.03	0.59	2.90	1.79	0.34	5.03	b
5	Gray <i>et al.</i> (2006)	3°	0.76–0.81	0.05	2500	1000	0.16	0.06	0.05	3.99	0.45	0.47	0.06	dep
6	Gray <i>et al.</i> (2006)	6°	0.76–0.81	0.11	2500	1000	0.11	0.06	0.07	3.99	0.45	0.17	0.05	dep
7	Gray <i>et al.</i> (2006)	9°	0.76–0.81	0.16	2500	1000	0.10	0.06	0.08	3.99	0.45	0.14	0.07	dep
8	Gray <i>et al.</i> (2005)	3°	1.00	0.05	2500	1000	0.16	0.06	0.07	3.99	0.45	0.23	0.03	dep
9	Gray <i>et al.</i> (2005)	6°	1.00	0.11	2500	1000	0.34	0.15	0.06	0.07	3.99	0.45	0.22	dep
10	Gray <i>et al.</i> (2005)	9°	1.00	0.16	2500	1000	0.34	0.13	0.06	0.07	3.99	0.45	0.21	dep
11	Eggenhuisen <i>et al.</i> (2019)	Run 1	2.3	0.14	2650	1000	0.10	7.91	0.65	2.90	1.79	0.30	7.26	b
12	Eggenhuisen <i>et al.</i> (2019)	Run 2	2.3	0.07	2650	1000	0.10	10.69	0.55	2.90	1.79	0.57	5.16	dep

Parameters listed are the measurement location at horizontal distance downstream of the inlet, X , bed slope, S , particle density, ρ_s , fluid density, ρ , flow depth, h , depth-averaged sediment concentration, c [%], depth-averaged velocity, u , median particle size, d_{50} , particle size standard deviation, σ , Richardson number, Ri , and Shields number, θ . The ‘flow regime’ indicates whether currents were reported to be accelerating (a), bypassing (b), decelerating (d) or depositional (dep).

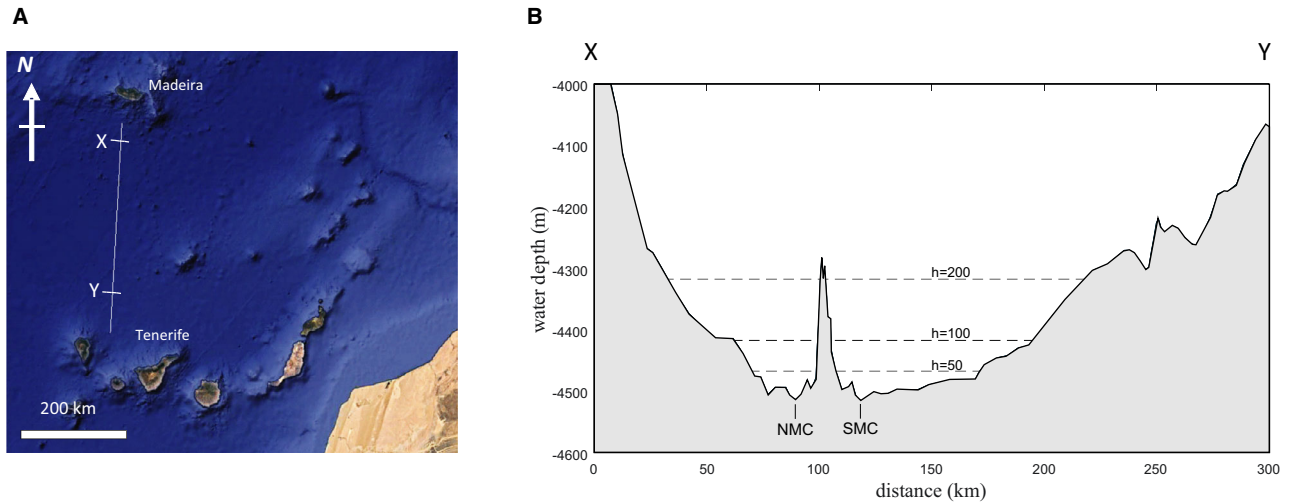


Fig. A2. (A) Location map of the North Atlantic. (B) North-south bathymetric profile along the transect shown in (A) crossing the Northern Madeira Channel (NMC), Southern Madeira Channel (SMC). Dashed lines indicate the possible widths of flows for different flow depths, h , assuming lateral spreading of currents to the basin margins. Map image and GEBCO bathymetric data from Google Earth©.

$$u_* = \sqrt{gRchS - \frac{a}{b+Ri} \left(1 + \frac{1}{2}Ri\right) u^2} \quad (\text{A4})$$

from which the Shields number is:

$$\theta = u_*^2 \rho / g \Delta \rho d_{50} \quad (\text{A5})$$

A4 PARTICLE SIZE DISTRIBUTION OF MADEIRA FLOWS

The particle-size distributions used in modelling of the Madeira Channel flows were taken from Stevenson *et al.* (2014): see their fig. 5. These data provide ‘total grain size distributions’ for event beds within the Madeira Abyssal Plain,

downstream of the Madeira Channel System, computed from measured grain-size distributions of samples from numerous seafloor cores. The distributions for Beds 5, 7 and 12 are shown in Fig. A1, which have median particle sizes of 5.1, 5.5 and 4.7 phi and standard deviations of 1.2, 1.3 and 1.3 phi, respectively.

A5 CROSS-SECTIONAL AREA OF MADEIRA CHANNEL FLOWS

The area of flows as a function of flow depth was calculated from integration of the area above the bathymetric profile along a transect orientated approximately north-south, perpendicular to the Madeira Channels (Fig. A2).